NASA CR-54726
SRI-I-TN-3

A FINITE DIFFERENCE SOLUTION FOR THE TWO-DIMENSIONAL EXPANSION OF A FINITE CYLINDRICAL GAS CLOUD INTO A VACUUM

by

G.G. BACH and J.H.S. LEE

prepared for

NATIONAL AERONAUTICS AND SPACE ADMINISTRATION

CONTRACT NAS 3-4190

SPACE RESEARCH INSTITUTE
McGILL UNIVERSITY

Requests for copies of this report should be referred to

National Aeronautics and Space Administration
Office of Scientific and Technical Information
Attention: AFSS-A
Washington, D.C. 20546

NASA CR-54726
SRI-I-TN-3

TOPICAL REPORT

A FINITE DIFFERENCE SOLUTION FOR THE TWO-DIMENSIONAL EXPANSION OF A FINITE CYLINDRICAL GAS CLOUD INTO A VACUUM

by

G.G. Bach and J.H.S. Lee

prepared for

NATIONAL AERONAUTICS AND SPACE ADMINISTRATION

April, 1966

CONTRACT NAS3-4190

Technical Management
NASA Lewis Research Center
Cleveland, Ohio
Liquid Rocket Technology Branch
Gordon T. Smith

SPACE RESEARCH INSTITUTE

McGill University
892 Sherbrooke St.W.
Montreal 2, Canada

SUMMARY

32190

The interaction of radial and axial rarefaction waves has been investigated by considering the expansion of a finite length cylindrical gas cloud into a vacuum. A numerical finite difference scheme was used for the integration of the basic conservation equations of gas dynamics. A "toral" co-ordinate system was developed for the solution of the flow in the "corner" regions of the cylinder. A perfect gas with $\gamma = 3$ was assumed and numerical results are given for three cases of radius to half length ratios greater than, equal to and less than unity. In spite of the simplicity of the physical model studied, experimental observations such as cloud shapes and the "indentations" made on witness plates downstream of the bumper are predicted by the present results.

FOREWORD

The results presented in this report constitute part of an overall theoretical research program on the hypervelocity impact of pellets on thin bumper plates. The work is sponsored by the Lewis Research Center of the National Aeronautics and Space Administration under contract NAS3-4190. The technical monitor is Mr. Gordon T. Smith.

The authors are grateful to Mr. I. Shanfield for his competent handling of all the programming and numerical calculations in this work, and to Dr. S.A. Gordon for constructive criticisms in the improvement of the report.

The important role played by Dr. G.V. Bull in the initiation of this study is also appreciated.

TABLE OF CONTENTS

LIST OF FIGURES

Page

1.0 INTRODUCTION

In the existing theoretical studies of hypervelocity impact phenomena by Bjork[1] and Walsh[2], the exact impact model has been tackled and elaborate computer codes have been developed to handle the problem in its entirety. Apart from the fact that considerable time and effort must be spent in developing these computer codes, this approach also suffers the disadvantage that it is not possible to determine the importance of, or the role played by, the various fundamental processes in the overall impact phenomenon.

A physical description of the end-on impact of cylindrical pellets with thin bumper plates has been given previously by Bull[3]. Subsequently, the fundamental processes of the one-dimensional radial and axial expansion of the condensed state generated by the impact shocks were studied in detail[4]. In the present report, the radial and axial expansion processes are coupled and the interaction of these two sets of rarefaction waves (i.e. radial and axial) are investigated.

In the present program of theoretical studies of end-on impact of cylindrical pellets with thin bumper plates, it was decided that a fresh approach should be taken. The impact phenomenon was first analyzed and then broken down into various fundamental processes, since it was believed that more fruitful results and a better understanding of the problem could be achieved in this manner. These physical processes were first studied individually and then progressively coupled together to form the complete impact model.

Upon actual meteoroid impact, it is assumed that the meteoroid and the impacted area of bumper will be vaporized forming a cylinder of highly compressed gas. This cylinder moves out from the bumper and begins to expand as the restraining medium is left behind. This report is an attempt to study analytically the expansion of this compressed cylinder of gas.

The physical model considered is the expansion of a cylindrical gas cloud of finite size, initially of diameter "$2R_0$" and length "$2L_0$". The cloud is shown in Figs. 1.1 (a) and (b) at time $t = 0$ and at time $t > 0$ respectively.

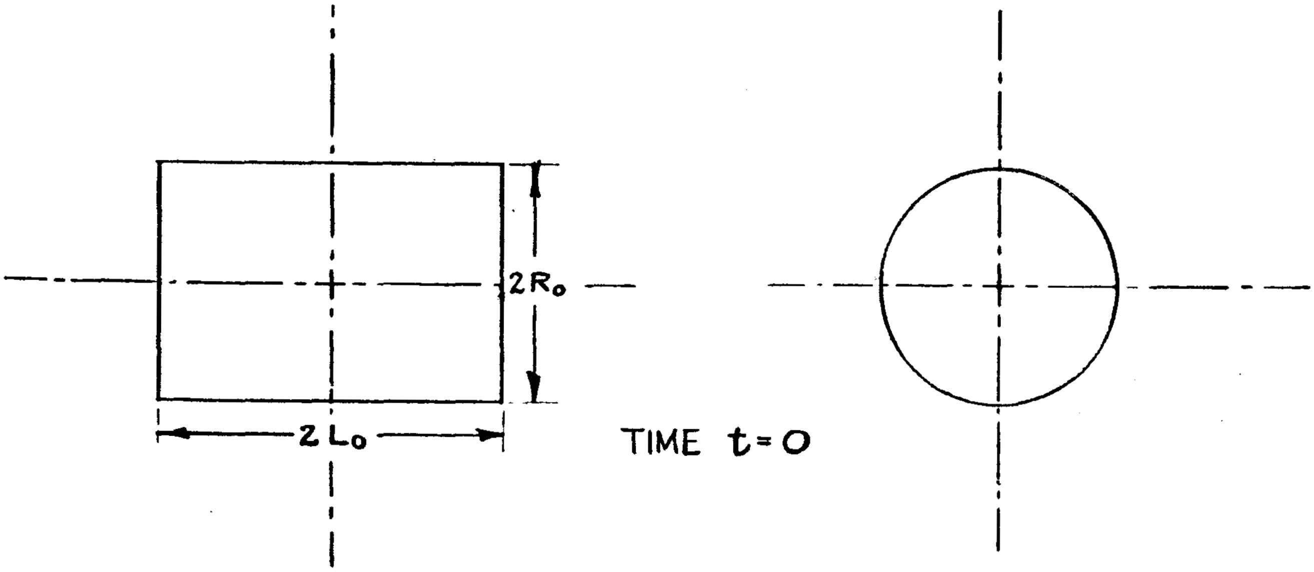

Figure 1.1 (a)

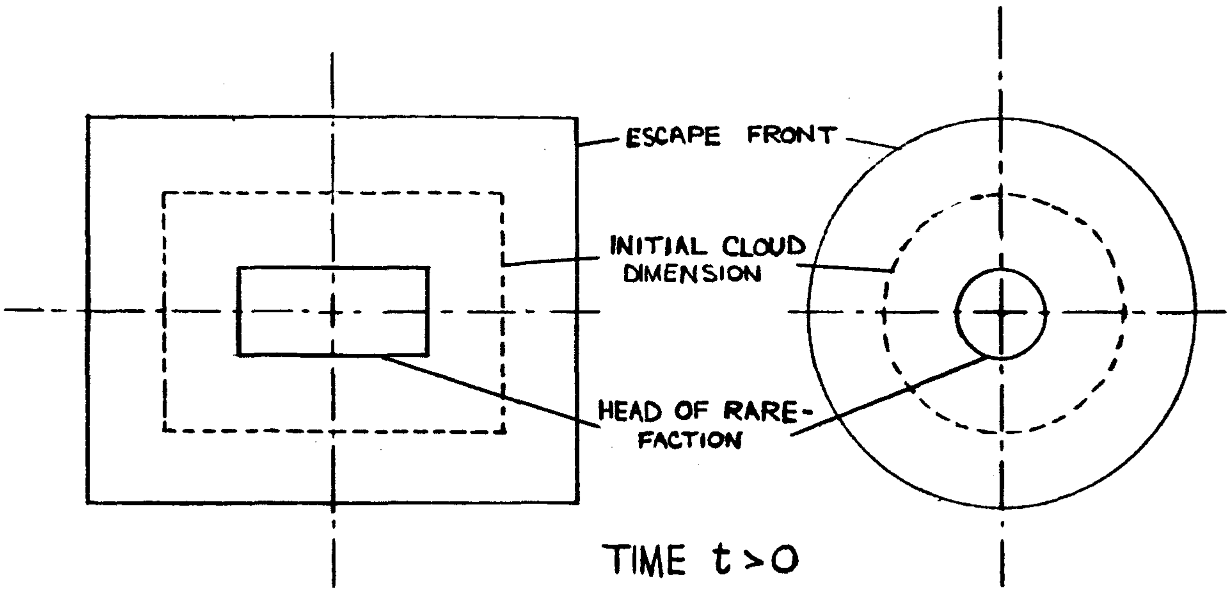

Figure 1.1 (b)

Depending on the ratio of the diameter to the length of the cylindrical gas cloud (i.e. R_o/L_o) the interaction processes are different. For example, if $R_o/L_o < 1$ (i.e. a long cylinder) the radial rarefaction wave will arrive at the axis of symmetry before the axial rarefaction waves (coming from the two ends) meet. For $R_o/L_o > 1$ (i.e. a short cylinder), the reverse is true. For a square cylinder ($R_o/L_o = 1$) both the axial and radial expansion waves converge at the center simultaneously. All three cases (i.e. $R_o/L_o < 1$, $R_o/L_o = 1$, and $R_o/L_o > 1$) are studied in the present work.

The expansion processes are assumed to be isentropic, with heat transfer, chemical and viscous effects being neglected. The gas cloud is taken to be uniform initially, and is assumed to act as a perfect gas with $\gamma = 3$.

The present problem, which involves two space co-ordinates as well as one time co-ordinate, cannot be solved analytically. Indeed, even for unsteady one-dimensional cylindrical or spherical expansions, analytical solutions of the similarity type exist only for non-uniform gas clouds with very special initial density distributions[5]. Instead, the expanding finite cylinder must be studied through exact numerical integration of the basic conservation equations. There are two possible numerical methods that can be adopted, the method of characteristics or a finite difference scheme. When the method of characteristics is used, the analysis involved is extremely complex since characteristic surfaces rather than characteristic lines have to be considered for a two-dimensional problem. A finite difference approach was therefore used in the present work.

2.0 THEORETICAL ANALYSIS

2.1 Basic Equations

In the absence of heat transfer and viscous effects, the conservation equations can be written as

Continuity $$\frac{D\rho}{Dt} + \rho \vec{\nabla} \cdot \vec{V} = 0 \tag{2.1}$$

Momentum $$\frac{D\vec{V}}{Dt} + \frac{1}{\rho} \vec{\nabla} p = 0 \tag{2.2}$$

Energy $$\frac{De}{Dt} + p \frac{D}{Dt}\left(\frac{1}{\rho}\right) = 0 \tag{2.3}$$

where ρ, p, e, and $\vec{V}$ are the density, pressure, energy and particle velocity respectively.

$\frac{D}{Dt}$ is the convective time derivative defined as

$$\frac{D}{Dt} \equiv \frac{\partial}{\partial t} + \vec{V} \cdot \vec{\nabla} . \tag{2.4}$$

For a perfect gas, the equation of state is given by

$$e = \frac{1}{\gamma - 1} \frac{p}{\rho} . \tag{2.5}$$

Using Eq. 2.5, the energy equation (Eq. 2.3) becomes

$$\left(\frac{\partial}{\partial t} + \vec{V} \cdot \vec{\nabla}\right) \frac{p}{\rho^\gamma} = \frac{D}{Dt}\left(\frac{p}{\rho^\gamma}\right) = 0 . \tag{2.6}$$

Eq. 2.6 merely states that the entropy for each fluid particle remains constant. Since the expansion process in the present problem is assumed to be isentropic throughout, Eq. 2.6 is satisfied automatically and the continuity and momentum equations are sufficient for the complete description of the expansion processes. However, for isentropic flow, it is more convenient to use the particle velocity and the local sound speed a as the dependent variables where a is defined by the relationship

$$a^2 = \frac{\partial p}{\partial \rho} . \tag{2.7}$$

The basic equations now become:

$$\frac{2}{\gamma - 1}\left(\frac{\partial a}{\partial t} + \vec{V}\cdot\vec{\nabla}a\right) + a\vec{\nabla}\cdot\vec{V} = 0 \tag{2.8}$$

$$\frac{\partial \vec{V}}{\partial t} + (\vec{V}\cdot\vec{\nabla})\vec{V} + \frac{2}{\gamma-1}a\vec{\nabla}a = 0 . \tag{2.9}$$

2.2 Flow Regions

For the analysis of the problem, only one quarter of the cylinder need be considered.

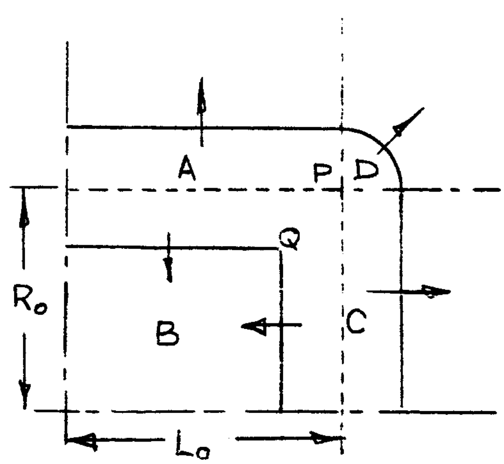

Shape of Expanding Gas Cloud

Figure 2.1

Originally, the cylinder has radius R_o and half length L_o, with the "corner" at P (Fig. 2.1a). This figure shows only one quarter of the cylinder. Later, when the expansion has proceeded for some time, the escape front (actually a surface) will have a shape as in Fig. 2.1b. It is interesting to note that the corner originally at P will now be at Q and will still be sharp since it is formed by the intersection of the radial and axial rarefaction fronts. A pictorial drawing of the entire cylindrical gas cloud after the expansion has proceeded for some time is shown in Fig. 2.2 below.

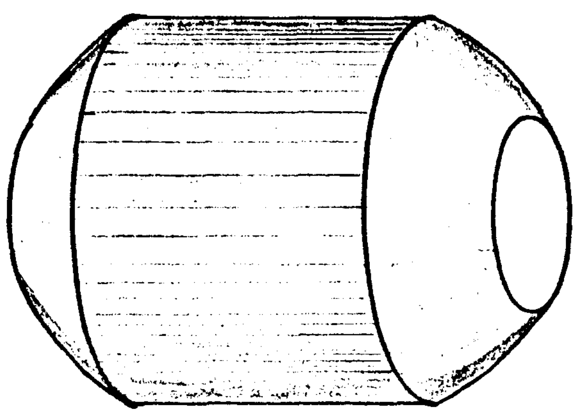

The Shape of An Expanding
Cylindrical Gas Cloud

Figure 2.2

From this model, it is clear that the cylindrical co-ordinate system is well suited for numerical solution of this problem, since the flow is axisymmetric. It was found, however, that it was more convenient to split the flow field into two regions and to use a different co-ordinate system for each region.

For the regions A, B and C, of Fig. 2.1 the cylindrical co-ordinates r and z were used, where r is the radial distance from the axis of the cylinder and z is the distance along the axis from the center.

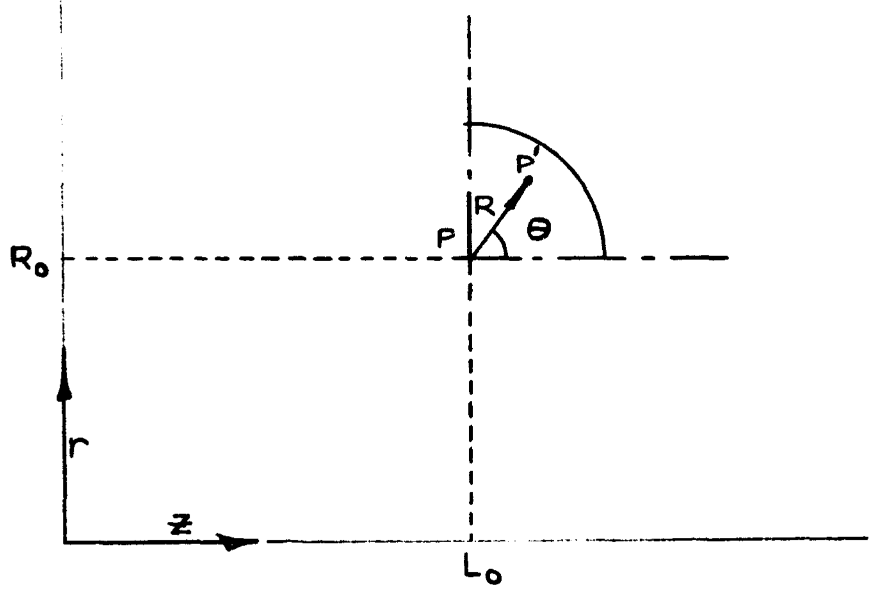

Figure 2.3

On the other hand, region D (the quarter-toroidal volume commencing at P) was found to be more conveniently analyzed using co-ordinates R and θ as shown in Fig. 2.3. It is seen that the surfaces, R = constant, generate tori with the common center line P of radius R_0. The surfaces θ = constant generate cones whose apexes lie on the axis of the cylinder. For brevity, this latter co-ordinate system will be referred to here as the "toral" co-ordinate system (not to be confused with the well known and quite different toroidal co-ordinate system). The general toral co-ordinate system is illustrated in Fig. 2.4.

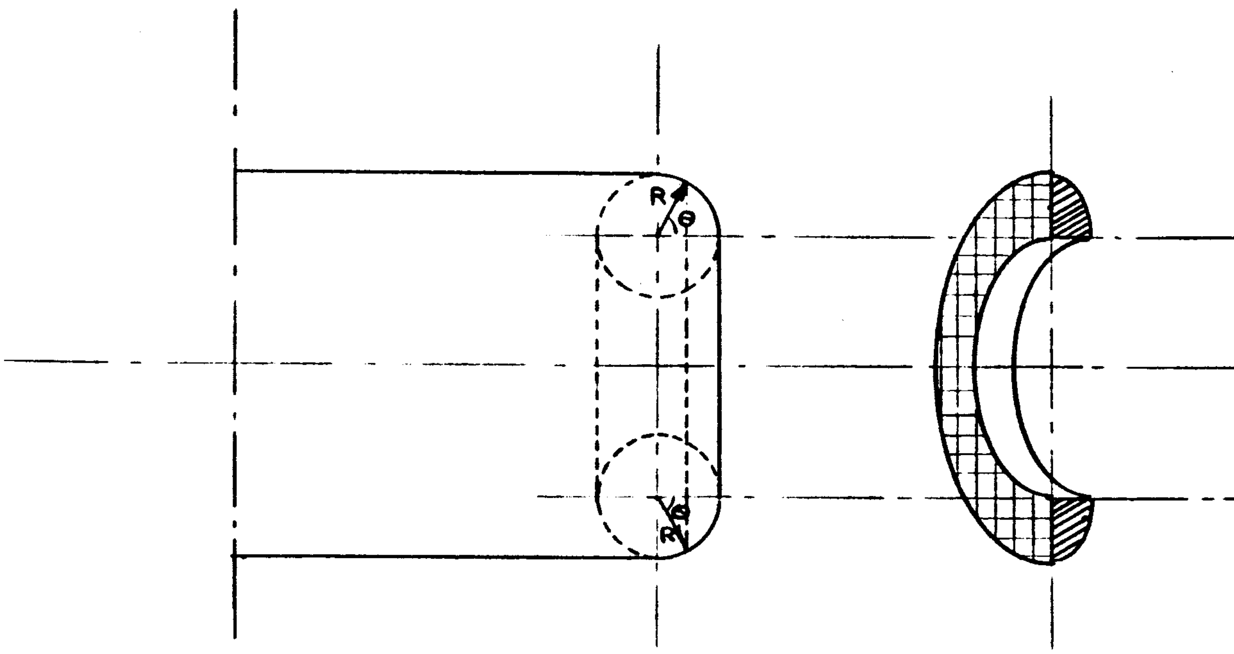

The Toral Co-ordinate System

Figure 2.4

The basic equations 2.8 and 2.9 can now be written in terms of cylindrical and toral co-ordinates.

a) Cylindrical Co-ordinates:

Let u and v be the components of the particle velocities in the axial and radial directions respectively. Then, in component form, Eqs. 2.8 and 2.9 become:

$$\frac{2}{\gamma-1}\left(\frac{\partial a}{\partial t}+v\frac{\partial a}{\partial r}+u\frac{\partial a}{\partial z}\right)+a\left(\frac{\partial v}{\partial r}+\frac{\partial u}{\partial z}+\frac{v}{r}\right)=0 \tag{2.10}$$

$$\frac{\partial v}{\partial t}+v\frac{\partial v}{\partial r}+u\frac{\partial v}{\partial z}+\frac{2}{\gamma-1}\,a\frac{\partial a}{\partial r}=0 \tag{2.11}$$

$$\frac{\partial u}{\partial t}+v\frac{\partial u}{\partial r}+u\frac{\partial u}{\partial z}+\frac{2}{\gamma-1}\,a\frac{\partial a}{\partial z}=0\,. \tag{2.12}$$

The above equations have been used everywhere in the flow field except in the part designated as Region D in Fig. 2.1b. For Region D the equations are written in terms of toral co-ordinates.

b) <u>Toral Co-ordinates</u>:

Referring to Figure 2.3, the transformation for a point P' from cylindrical to toral co-ordinates is

$$\begin{aligned} r &= R_o + R\sin\theta \\ z &= L_o + R\cos\theta\,. \end{aligned} \tag{2.13}$$

The partial derivatives $\frac{\partial}{\partial r}$ and $\frac{\partial}{\partial z}$ in terms of toral co-ordinates are

$$\frac{\partial}{\partial r}=\frac{\partial R}{\partial r}\frac{\partial}{\partial R}+\frac{\partial\theta}{\partial r}\frac{\partial}{\partial\theta} \tag{2.14}$$

$$\frac{\partial}{\partial z}=\frac{\partial R}{\partial z}\frac{\partial}{\partial R}+\frac{\partial\theta}{\partial z}\frac{\partial}{\partial\theta}\,. \tag{2.15}$$

From Eqs. 2.13, one obtains

$$R=\left[(z-L_o)^2+(r-R_o)^2\right]^{\frac{1}{2}}\,. \tag{2.16}$$

Using Eq. 2.16, Eqs. 2.14 and 2.15 become:

$$\begin{aligned} \frac{\partial}{\partial r} &= \sin\theta\frac{\partial}{\partial R}+\frac{\cos\theta}{R}\frac{\partial}{\partial\theta} \\ \frac{\partial}{\partial z} &= \cos\theta\frac{\partial}{\partial R}-\frac{\sin\theta}{R}\frac{\partial}{\partial\theta}\,. \end{aligned} \tag{2.17}$$

Substituting Eqs. 2.17 into Eqs. 2.10, 2.11, and 2.12, the conservation equations become:

MASS CONSERVATION:

$$\frac{2}{\gamma-1}\left[\frac{\partial a}{\partial t}+\sin\theta\left(v\frac{\partial a}{\partial R}-\frac{u}{R}\frac{\partial a}{\partial\theta}\right)+\cos\theta\left(u\frac{\partial a}{\partial R}+\frac{v}{R}\frac{\partial a}{\partial\theta}\right)\right]$$
$$+a\left[\sin\theta\left(\frac{\partial v}{\partial R}-\frac{1}{R}\frac{\partial u}{\partial\theta}\right)+\cos\theta\left(\frac{\partial u}{\partial R}+\frac{1}{R}\frac{\partial v}{\partial\theta}\right)+\frac{v}{R_o+R\sin\theta}\right]=0 \tag{2.18}$$

MOMENTUM CONSERVATION in the r direction:

$$\frac{\partial v}{\partial t}+\sin\theta\left(v\frac{\partial v}{\partial R}-\frac{u}{R}\frac{\partial v}{\partial\theta}\right)+\cos\theta\left(u\frac{\partial v}{\partial R}+\frac{v}{R}\frac{\partial v}{\partial\theta}\right)$$
$$-\frac{2}{\gamma-1}\,a\left(\sin\theta\frac{\partial a}{\partial R}+\frac{\cos\theta}{R}\frac{\partial a}{\partial\theta}\right)=0 \tag{2.19}$$

MOMENTUM CONSERVATION in the z direction:

$$\frac{\partial u}{\partial t}+\sin\theta\left(v\frac{\partial u}{\partial R}-\frac{u}{R}\frac{\partial u}{\partial\theta}\right)+\cos\theta\left(u\frac{\partial u}{\partial R}+\frac{v}{R}\frac{\partial u}{\partial\theta}\right)$$
$$+\frac{2}{\gamma-1}\,a\left(\cos\theta\frac{\partial a}{\partial R}-\frac{\sin\theta}{R}\frac{\partial a}{\partial\theta}\right)=0 \tag{2.20}$$

2.3 Initial and Starting Conditions

Based on the physical model described in Section 1, the initial conditions of the cylindrical gas cloud are:

$a = a_o$, $\quad \vec{V} = 0$ for $\quad z \leq L_o$, $\quad r \leq R_o$

and $\quad a = 0$, $\quad \vec{V} = 0$ elsewhere

at time $t = 0$.

Since initially, the density of the cylindrical gas cloud is uniform, the gradient of the sound speed "a" is infinite at the boundary $z = L_o$ and $r = R_o$. It is therefore not possible to start the numerical integration of Eqs. 2.10 to 2.12 with these initial conditions.

The expansion of the gas cloud for the first time increment, however, may be approximated by a planar solution, since in the z -direction, this is actually the case, and in the r -direction, such an approximation led to satisfactory results in a previous study[4]. In addition, the singularities which exist at the corner of the cylinder can be eliminated by assuming that the corner possesses a small radius of curvature. The curvature effects, even in the corner region, can be neglected, since it was previously found[4] that the overall flow field is rather insensitive to the starting conditions. These starting conditions at the first time increment may now be found.

Because of these considerations, the initial cloud geometry was slightly modified. It was assumed to be of radius $R_0 + a_0\Delta$ and half length $L_0 + a_0\Delta$ with corners of radius of curvature of $a_0\Delta$. After a small time interval Δ has elapsed, the flow field will be as shown in Fig. 2.5.

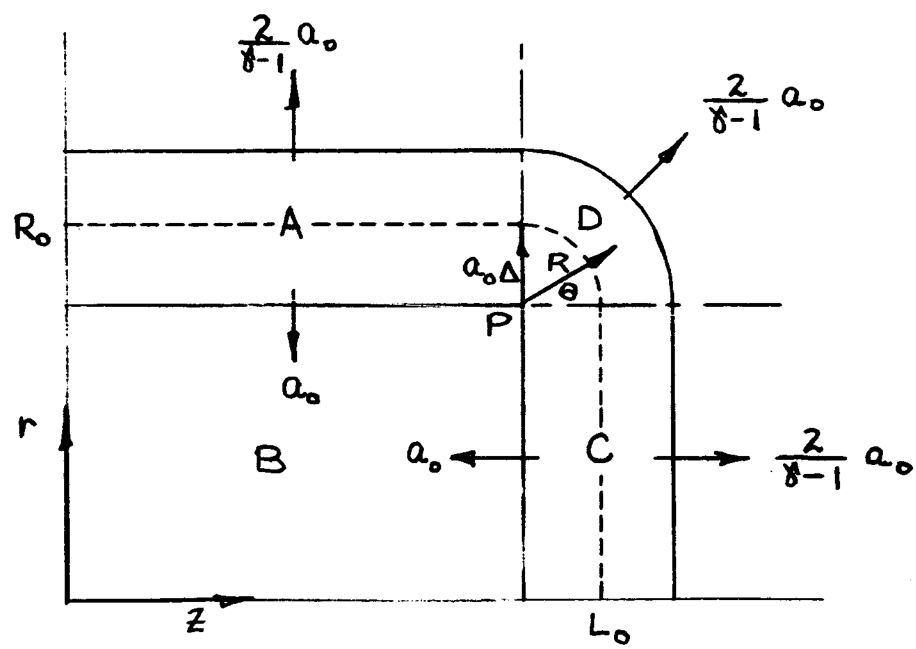

Figure 2.5

The radial expansion in region A was treated as planar similar to the axial expansion in region C during the small time interval Δ . The distributions of the particle velocity and the sound speed with radial and axial distances after the expansion has proceeded for a time $t = \Delta$ can be obtained readily by the method of characteristics as described in Ref. 4. They are:

In region A $(0 \leq z \leq L_o)$,

for $\quad 0 < r < R_o , \qquad \begin{cases} a = a_o \\ u = v = 0 \end{cases}$;

$$\text{for} \quad R_o \leq r \leq R_o + \frac{\gamma+1}{\gamma-1} a_o \Delta , \quad \begin{cases} a = a_o - \dfrac{\gamma-1}{\Delta(\gamma+1)} (r - R_o) \\ u = 0 \\ v = \dfrac{2}{\Delta(\gamma+1)} (r - R_o) \quad ; \end{cases} \tag{2.21}$$

for $\quad r > R_o + \frac{\gamma+1}{\gamma-1} a_o \Delta , \qquad a = u = v = 0 .$

In region C $(0 \leq r \leq R_o)$,

for $\quad 0 < z < L_o , \qquad \begin{matrix} a = a_o \\ u = v = 0 \end{matrix}$;

$$\text{for} \quad L_o \leq z \leq L_o + \frac{\gamma+1}{\gamma-1} a_o \Delta , \quad \begin{matrix} a = a_o - \dfrac{\gamma-1}{\Delta(\gamma+1)} (z - L_o) \\ u = \dfrac{2}{\Delta(\gamma+1)} (z - L_o) \\ v = 0 \quad ; \end{matrix} \tag{2.22}$$

for $\quad z > L_o + \frac{\gamma+1}{\gamma-1} a_o \Delta , \qquad a = u = v = 0 .$

For smooth transition from region A to region C, the starting conditions in the corner region D were assumed to be identical to those in regions A and C as given by Eqs. 2.21 and 2.22. This assumption guaranteed a matching of the flow variables in all three regions. In toral co-ordinates, the starting condition for region D can be written as

$$0 \leq R \leq \frac{\gamma+1}{\gamma-1} a_o \Delta \qquad \left\{ \begin{aligned} a &= a_o - \frac{\gamma-1}{\Delta(\gamma+1)} R \\ u &= \frac{2}{\Delta(\gamma+1)} R \cos\theta \\ v &= \frac{2}{\Delta(\gamma+1)} R \sin\theta \,. \end{aligned} \right. \qquad (2.23)$$
$$0 \leq \theta \leq \frac{\pi}{2}$$

It is seen that when $\theta = \frac{\pi}{2}$ and $\theta = 0$, Eqs. 2.23 reduce to Eqs. 2.21 or 2.22 or regions A and C respectively. With the starting conditions now determined, (Eqs. 2.21, 2.22 and 2.23) the basic conservation equations (Eqs. 2.10 to 2.12 and Eqs. 2.18 to 2.20) can be integrated numerically by a finite difference scheme.

2.4 Selection of the Mesh

For the finite difference numerical calculation, the expansion flow field was replaced by a mesh of lattice points as shown in Fig. 2.6. Except in region D, a "square" grid with mesh size h was used. A "circular" grid was devised for region D as shown in Fig. 2.6. In this region, the mesh point (i,j) is given by the toral co-ordinates

$$\begin{aligned} R(i,j) &= ih \\ \theta(i,j) &= \frac{\pi}{2} \cdot \frac{j}{i} \,. \end{aligned} \qquad (2.24)$$

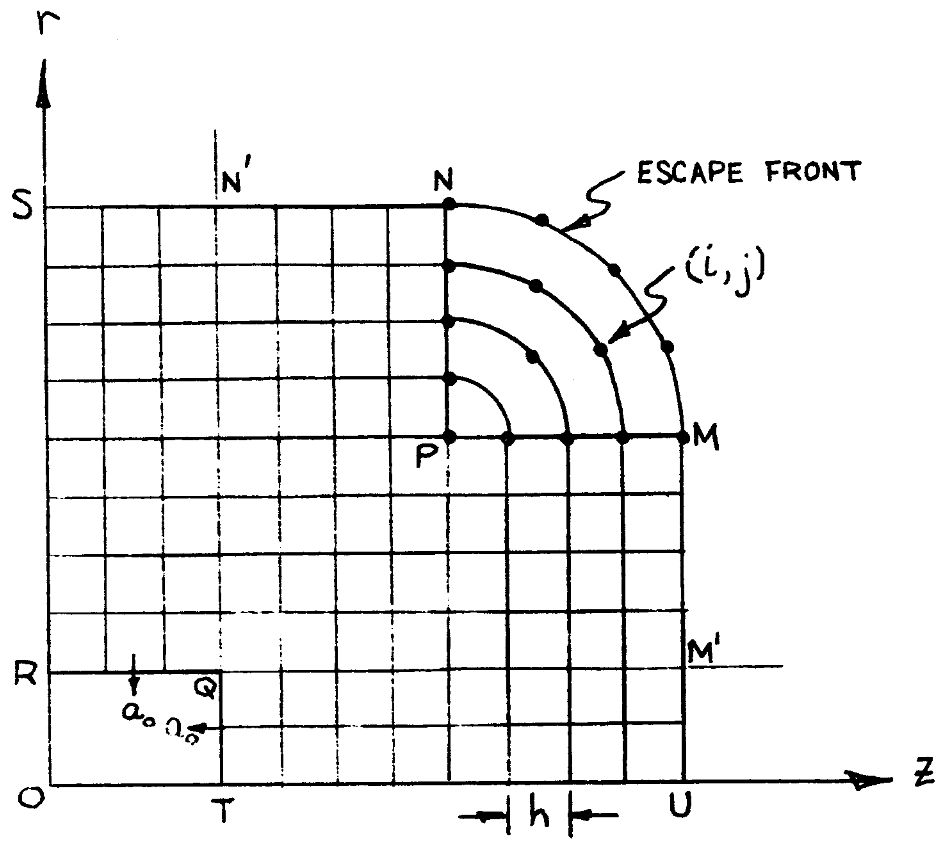

Figure 2.6

With the choice of mesh as given by Eqs. 2.24, $\Delta R = h$ and $R \Delta \theta = \frac{\pi h}{2}$ so that the same form of difference equation applied everywhere in the toral region.

2.5 The Difference Equations

For the square mesh region (See Fig. 2.6) the partial derivatives of a flow variable $f(r, z, t)$ were approximated by the following centered differences:

$$\frac{\partial f}{\partial r}(r,z,t) \cong \frac{f(r+h,z,t)-f(r-h,z,t)}{2h} \tag{2.25}$$

$$\frac{\partial f}{\partial z}(r,z,t) \cong \frac{f(r,z+h,t)-f(r,z-h,t)}{2h} \tag{2.26}$$

$$\frac{\partial f}{\partial t}(r,z,t) \cong \frac{1}{\Delta t}\Big[f(r,z,t+\Delta t)-\frac{1}{4}\Big\{f(r+h,z,t)+f(r-h,z,t) + f(r,z+h,t)+f(r,z-h,t)\Big\}\Big]. \tag{2.27}$$

Substitution of Eqs. 2.25, 2.26 and 2.27 into the basic equations (Eqs, 2.10, 2.11 and 2.12) resulted in explicit forms for the solutions of the properties at the new time $t+\Delta t$ in terms of the properties at the previous time t .

In the toral region D, the derivatives of a property f at the mesh point (i,j) were taken to be:

$$\frac{\partial f}{\partial R}(i,j,t) \cong \frac{1}{2ih}\Big[jf(i+1,j+1,t)+(i-j)f(i+1,j,t) - jf(i-1,j-1,t)-(i-j)f(i-1,j,t)\Big] \tag{2.28}$$

$$\frac{1}{R}\frac{\partial f}{\partial \theta}(i,j,t) \cong \frac{1}{\pi h}\Big[f(i,j+1,t)-f(i,j-1,t)\Big] \tag{2.29}$$

$$\frac{\partial f}{\partial t}(i,j,t) \cong \frac{1}{\Delta t}\Big[f(i,j,t+\Delta t)-\frac{1}{2i}\Big\{jf(i+1,j+1,t) + (i-j)f(i+1,j,t)+jf(i-1,j-1,t)+(i-j)f(i-1,j,t)\Big\}\Big]. \tag{2.30}$$

By substituting the above equations into the basic equations (Eqs. 2.18, 2.19 and 2.20), explicit relations were obtained for the determination of the flow variables at the next time step.

Since a perfect gas with γ = 3 was assumed throughout the present study, both the escape front and the head of the rarefaction front propagate at the same velocity, equal to the initial undisturbed sound speed a_o. To ensure stability, the space-time mesh ratio was taken as[6]:

$$\frac{h}{\Delta t} = a_o \quad (2.31)$$

It should be mentioned that the choice of the toral mesh was partially dictated by stability conditions. From Eqs. 2.24 and 2.31, one obtains

$$\frac{\Delta R}{\Delta t} = a_o$$

$$R\frac{\Delta\theta}{\Delta t} = \frac{\pi}{2} a_o$$

which satisfy the stability requirements. From Eq. 2.31, one readily sees that with each time step, new rows of mesh points lie on the new escape and rarefaction fronts. This simplifies the numerical calculations.

Referring to Fig. 2.6, where the meshed region (including region D) represents the entire flow field at any instant of time, it can be seen that the only part of the flow field containing two-space dimensional effects is the area bounded by the lines QN', QM' and the escape front N'NMM'. This is the region where the interaction of the radial and axial rarefaction waves occurs. The region QN'SR is a purely one-dimensional cylindrical expansion while region QTUM' is a one-dimensional planar expansion investigated previously[4].

3.0 RESULTS AND DISCUSSION

Whether the axial or radial rarefaction dominates the overall expansion of the cylindrical gas cloud depends on the geometry of the cloud itself (i.e. the ratio R_o/L_o). For example, the expansion of a cylindrical cloud with $R_o/L_o > 1$ will be mainly axial, while for $R_o/L_o < 1$, the expansion will be mainly radial. Numerical computations have been performed for all three cases; a long cylinder $R_o/L_o = 1/2$, a square cylinder $R_o/L_o = 1$ and a short cylinder $R_o/L_o = 2$.

All the numerical results presented in the present study are based on a value of $\gamma = 3$. In a previous study[4], it was found that using $\gamma = 3$, the one-dimensional cylindrical expansion field of condensed aluminum processed by a strong shock of density ratio $\frac{\rho_1}{\rho_0} = 2$ can be described accurately. Hence, in the present study of expansions involving two-space dimensions, numerical calculations using Tillotson's equation of state were not performed again, since the effect of the equation of state on the expansion flow field had already been determined in the previous work[4] on one-dimensional expansion. This illustrates one of the advantages of the stepwise approach adopted in this study.

For isentropic flow, two flow variables are sufficient for the complete determination of the flow field. The present study used the sound speed a and the particle velocity $\vec{V}$ as the two flow variables. With the sound speed known, the density, pressure and internal energy can be found directly from the isentropic relationships

$$\frac{a}{a_o} = \left(\frac{\rho}{\rho_o}\right)^{\frac{\gamma-1}{2}} = \left(\frac{p}{p_o}\right)^{\frac{\gamma-1}{2\gamma}} = \left(\frac{e}{e_o}\right)^{\frac{1}{2}} \qquad (3.1)$$

where the subscript o denotes the initial conditions.

All the numerical results presented are in dimensionless form. The dependent variables a, u, and v are non-dimensionalized with respect to a_o. The independent variables t, r, and z are non-dimensionalized as follows:

$$\text{For} \quad \frac{R_o}{L_o} \geq 1 \qquad \begin{cases} t = \dfrac{a_o t'}{R_o} \\ r = \dfrac{r'}{R_o} \\ z = \dfrac{z'}{R_o} \end{cases}$$

$$\text{For} \quad \frac{R_o}{L_o} < 1 \qquad \begin{cases} t = \dfrac{a_o t'}{L_o} \\ r = \dfrac{r'}{L_o} \\ z = \dfrac{z'}{L_o} \end{cases}$$

where the primed quantities have dimensions.

The variation of the sound speed a and the particle velocity $\vec{V}$ with radial and axial distances at different times t for the three geometries (i.e. $R_o/L_o < 1$, $R_o/L_o = 1$, and $R_o/L_o > 1$) are given in Figs. 3.1 to 3.12.

Due to the two-dimensional geometry of the gas cloud, it is difficult to make meaningful quantitative comparisons between the present results and those obtained previously for purely planar, cylindrical and spherical expansion. However, on a qualitative basis, the interaction of radial and axial rarefaction waves can be demonstrated by the shapes of the various sound speed profiles. For example, at all times the distribution of the sound speed for one-dimensional planar expansions are monotonic functions of the space variable "x", decreasing smoothly from its value at the center line to zero at the escape front. Referring to Fig. 3.9, where the distributions of the sound speed along the z axis for a short cylinder ($R_o/L_o = 2$) at various times are shown, one can see that before the effect of the radial expansion is "felt" at the z axis, the sound speed a decreases monotonically from its value at the center to zero at the escape front, identical to the one-dimensional planar expansion case. As the radial rarefaction waves reach the z axis, material is escaping in a radial direction as well as in the axial direction. This results in a flattening of the sound speed (or density) profiles near the center of the gas cloud as shown in Fig. 3.9. Since the rate at which mass is escaping is higher for radial rarefactions than for axial rarefactions, an anomalous "bump" is developed in the density profiles which finally smooths out at large times.

The effect of the interaction between radial and axial rarefaction waves on the center line distributions are qualitatively similar for all the three cases studied (i.e. $R_o/L_o < 1$, $R_o/L_o = 1$ and $R_o/L_o > 1$). A comparison of the axial density profiles for the three cases at a value of t when the axial escape front has traversed a distance of $2L_o$ is shown in Fig. 3.13. The higher rate of "mass ejection" by the radial rarefactions in the case of $R_o/L_o < 1$ is demonstrated by the much more rapid density and speed of sound decay in the case of $R_o/L_o = 1/2$.

Due to the two-dimensional nature of the present problem, the interaction of radial and axial rarefaction waves cannot be effectively demonstrated by the center-line distribution shown in Fig. 3.1 to 3.12, and a two-dimensional plot is required. In Fig. 3.14, constant sound speed contours (or constant density contours since for $\gamma = 3$, $a = \rho$) for a square cylinder are plotted at that instant of time when the escape front has moved a distance of $2R_o$. The shape of the escape front is shown as a dotted line and the density profiles through three sections of the expansion field are also plotted. Two interesting observations can be made from Fig. 3.14. Because the density of the material near the escape front is extremely low and changing density slowly, the boundary of the expanding cloud shown in the shadowgraphs obtained experimentally by the Beckman-Whitley high speed framing camera is probably that of the higher-density contours. A typical shadowgraph of an expanding cloud is shown in Fig. 3.15 and as can be observed, the cloud boundary is similar to that of the .01 or .04 constant density contour of Fig. 3.14. This indicates that the particular shape of the expanding cloud as observed experimentally is compatible with the theoretical prediction given here.

Another interesting observation is the non-uniform change of density in the expansion field which results from the interaction of radial and axial rarefaction waves. (For purely one-dimensional expansion, the density decreases uniformly from the center of the cloud to the escape front.) This non-uniform density variation could produce the ring-shaped indentations which have been observed on a witness plate downstream of the bumper.

The mass distribution profile in the radial direction through section BB as shown in Fig. 3.14 clearly indicates that a concentration of mass exists near the periphery of the cloud.

The direction and the magnitude of the particle velocity on a particular surface in the expansion field for a square cylinder ($^{R_o}/_{L_o} = 1$) and a short cylinder ($^{R_o}/_{L_o} > 1$) are shown in Figs. 3.16 and 3.17 respectively. As can be seen, the direction of the particle velocity gradually changes from the axial direction on the z axis to the radial direction on the r axis, while its magnitude is almost constant along the surface. This indicates that, in spite of the fact that the density variation is non-uniform, the mass flow from the expanding cylinder is almost symmetrical with respect to its original shape.

4.0 CONCLUDING REMARKS

Perhaps the most important conclusion that can be drawn from the results of the present study is that the initial geometrical shape of the gas cloud strongly influences the resultant expansion field. Due to the different rates of expansion in the radial and the axial direction, a non-uniform distribution of mass occurs in the expanding cloud. This non-uniformity cannot be explained by purely one-dimensional considerations. In spite of the simplicity of the present physical model, the results shed considerable light on some of the experimental observations made as previously discussed.

The present development could be refined by removing the approximation made in determining the starting conditions as described in Section 2.3. Such an investigation would provide quantitative results of the effect of starting profiles on the subsequent flow field at later times and would be of interest to future studies of hypervelocity impact problems involving three space variables. Also, the study of the interaction of spherical and cylindrical rarefactions by considering the expansion of a cylinder with hemi-spherical ends and the expansion of gas clouds of arbitrary shapes is not only of academic interest, but also of practical interest in the study of end-on and oblique impacts of pellets of arbitrary shape.

REFERENCES

1. Bjork, R.L.
"Effects of a Meteoroid Impact on Steel and Aluminum in Space"
(Springer-Verley, 1960)
Vol. II 505-514

2. Walsh, J.M. and Tillotson, J.H.
"Hydrodynamics of Hypervelocity Impact"
Proc. of the sixth sym. on Hypervelocity Impact
Vol. 2 Pt. 1, pp 59-104 (Aug. 1963)

3. Bull, G.V.
"On the Impact of Pellets with Thin Plates"
McGill University
T.N. 1-10/61 (1961)

4. Shanfield, I., Lee, J.H., and Bach, G.G.
"A Finite-Difference Solution for the Cylindrical Expansion of a Gas Cloud into a Vacuum"
NASA CR-54254 (March 1965)

5. Keller, J.B.
"Spherical Cylindrical and One-Dimensional Gas Flows"
Quart. Appl. Math 14, 171-184 (1957)

6. Richtmyer, R.D.
"Difference Methods for Initial-Value Problems"
Wiley (Interscience), New York 1957

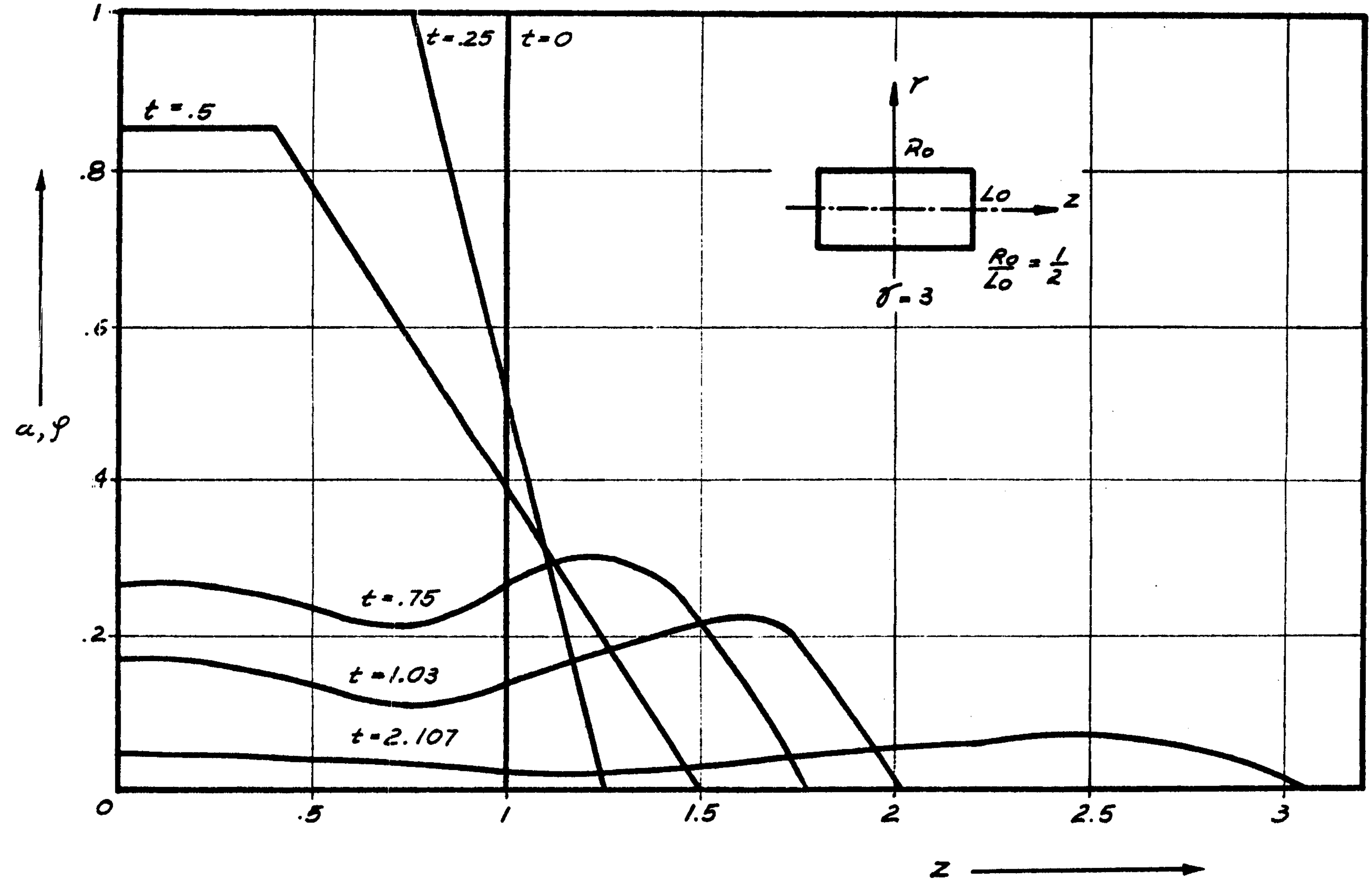

FIG. 3.1 SOUND SPEED PROFILES FOR LONG CYLINDER ALONG Z AXIS

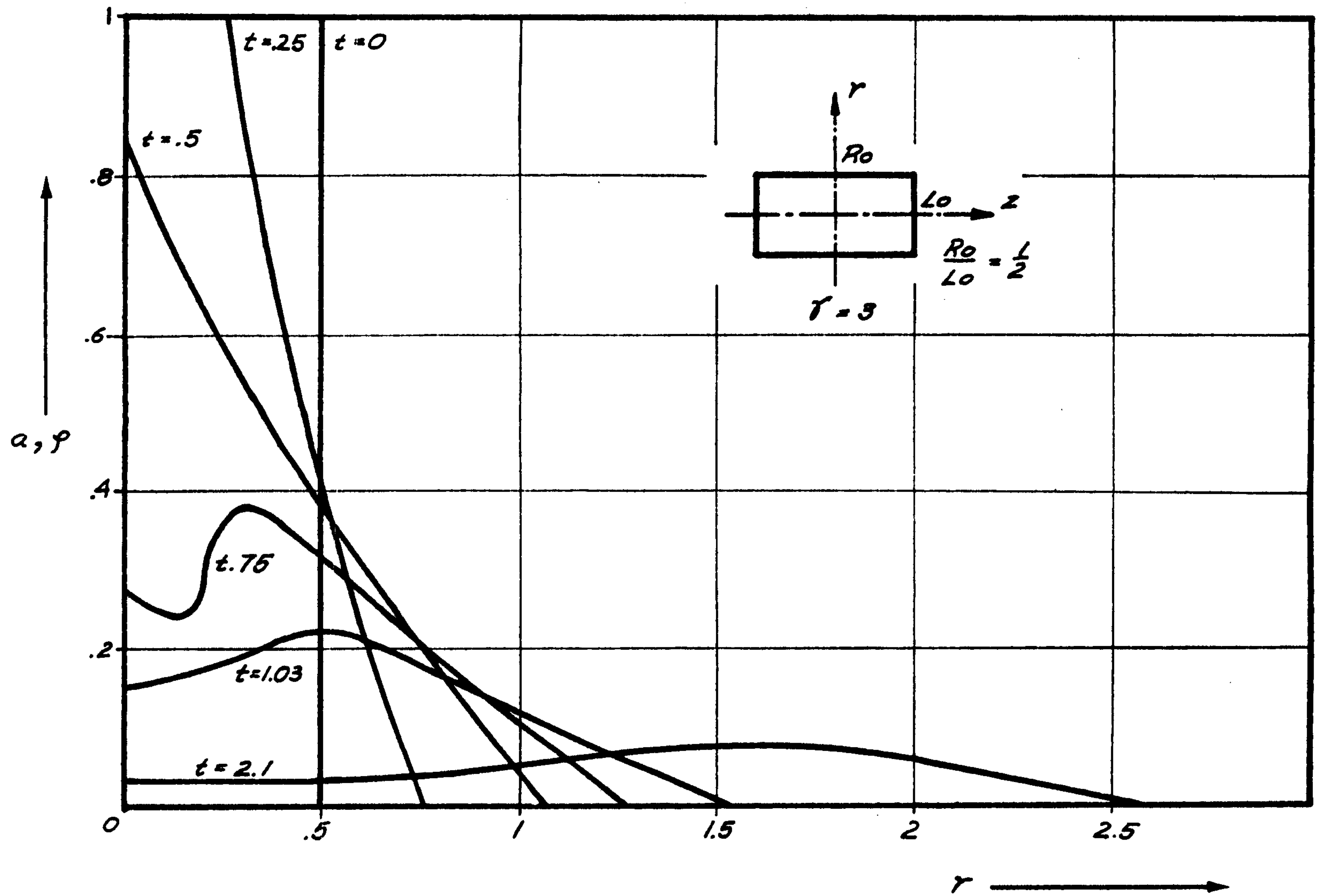

FIG. 3.2 SOUND SPEED PROFILES FOR LONG CYLINDER ALONG r AXIS

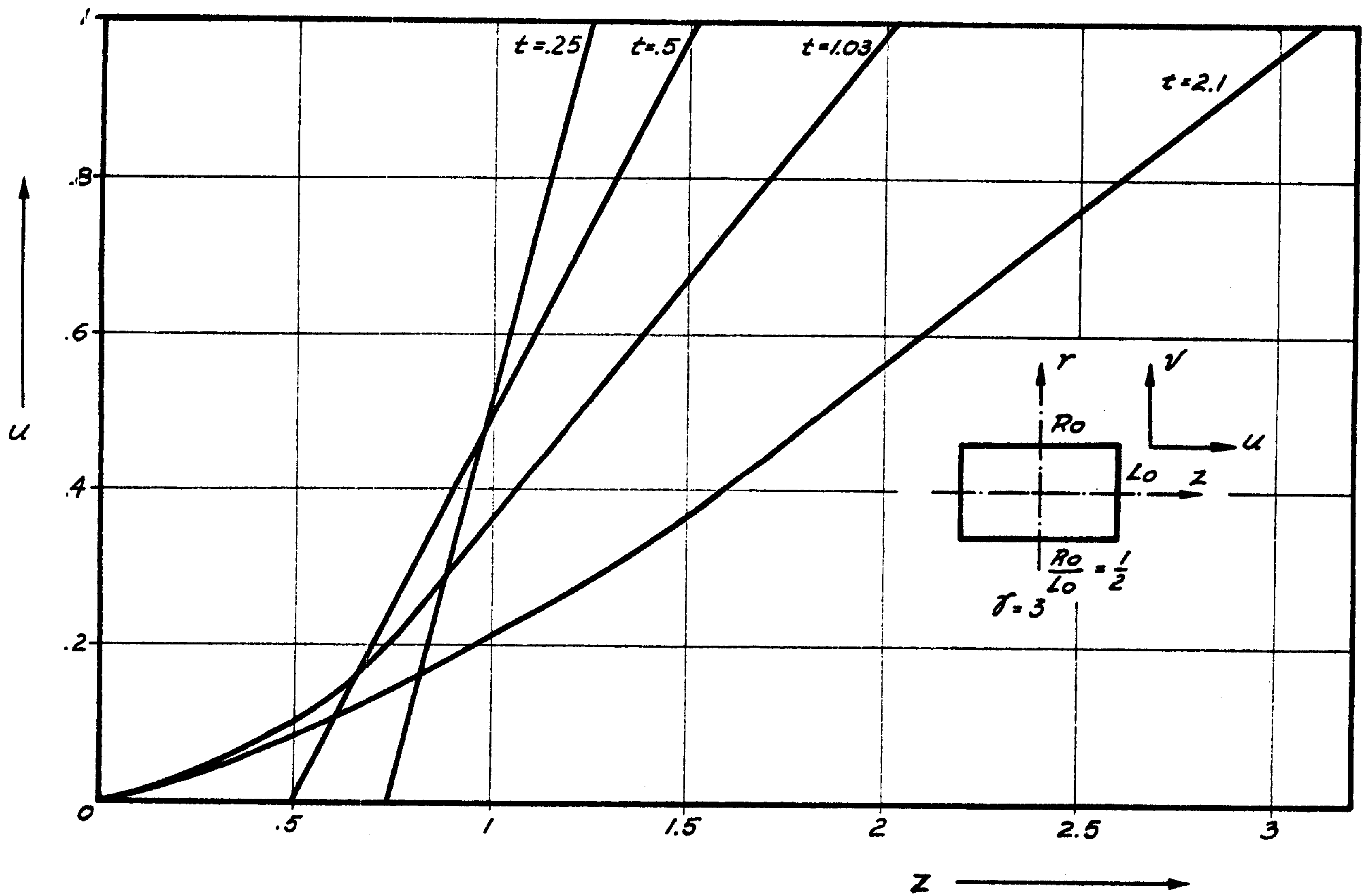

FIG. 3.3 PARTICLE VELOCITY PROFILES FOR LONG CYLINDER ALONG Z AXIS

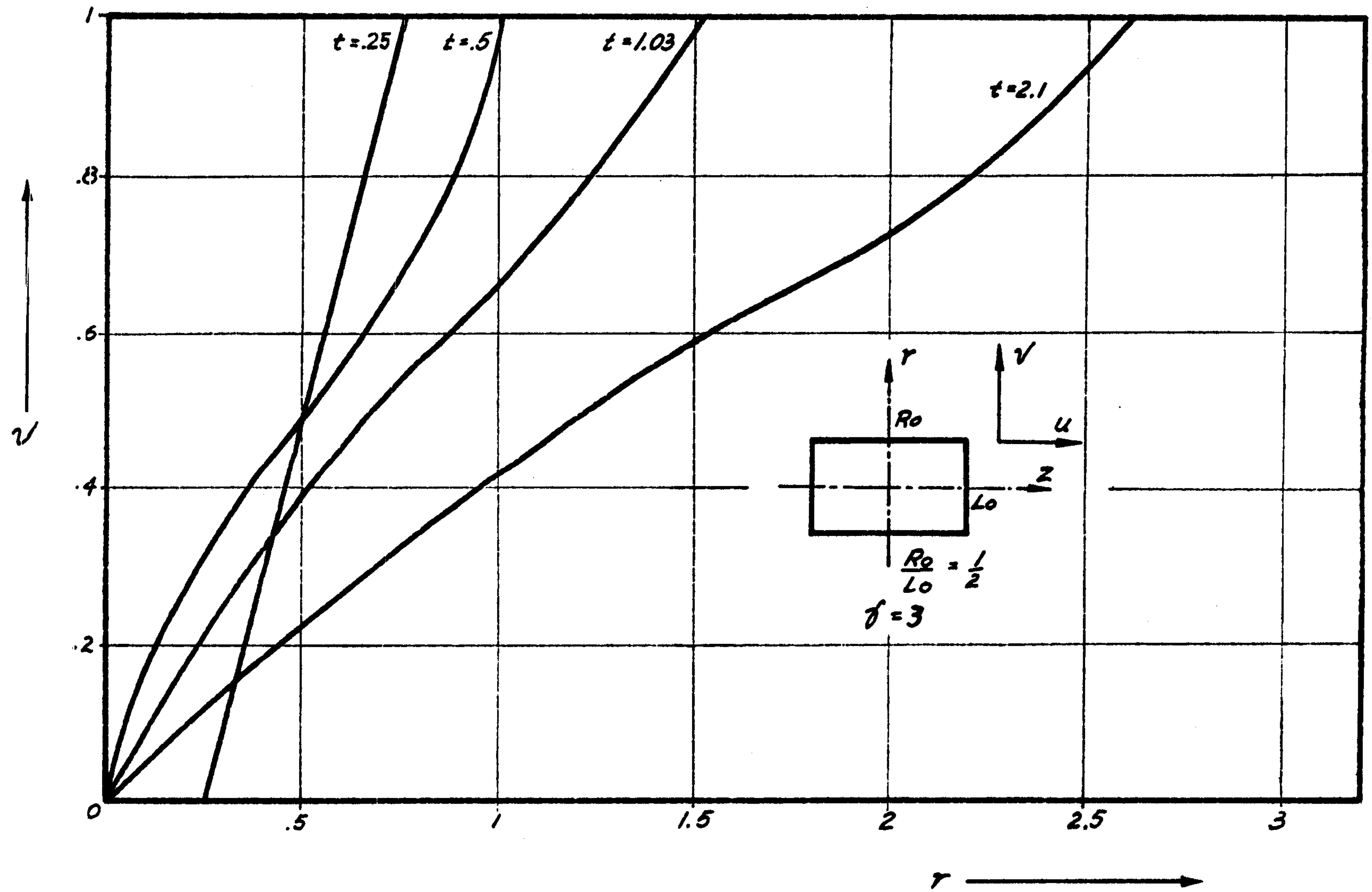

FIG. 3.4 PARTICLE VELOCITY PROFILES FOR LONG CYLINDER ALONG r AXIS

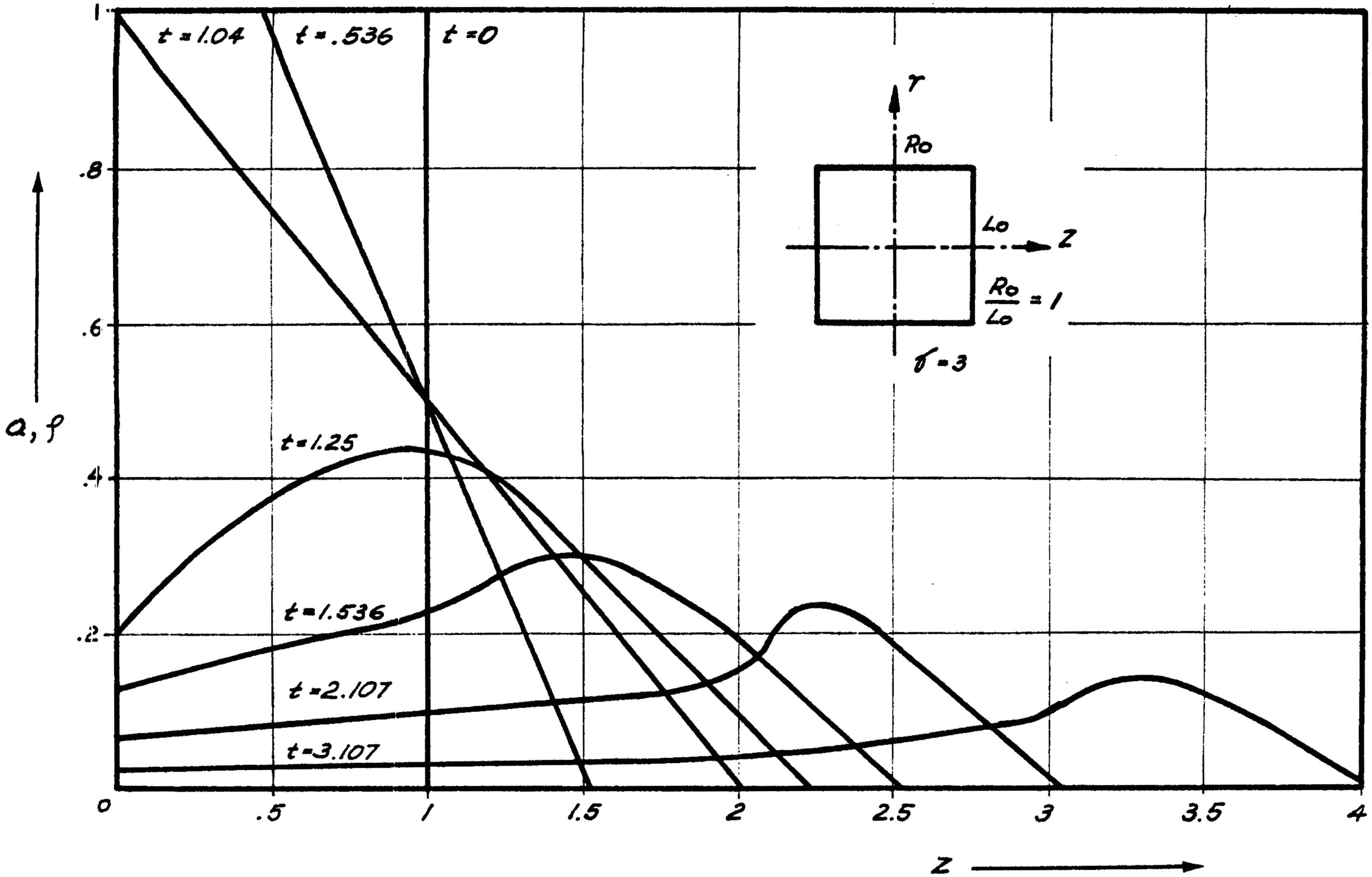

FIG. 3.5 SOUND SPEED PROFILES FOR SQUARE CYLINDER ALONG Z AXIS

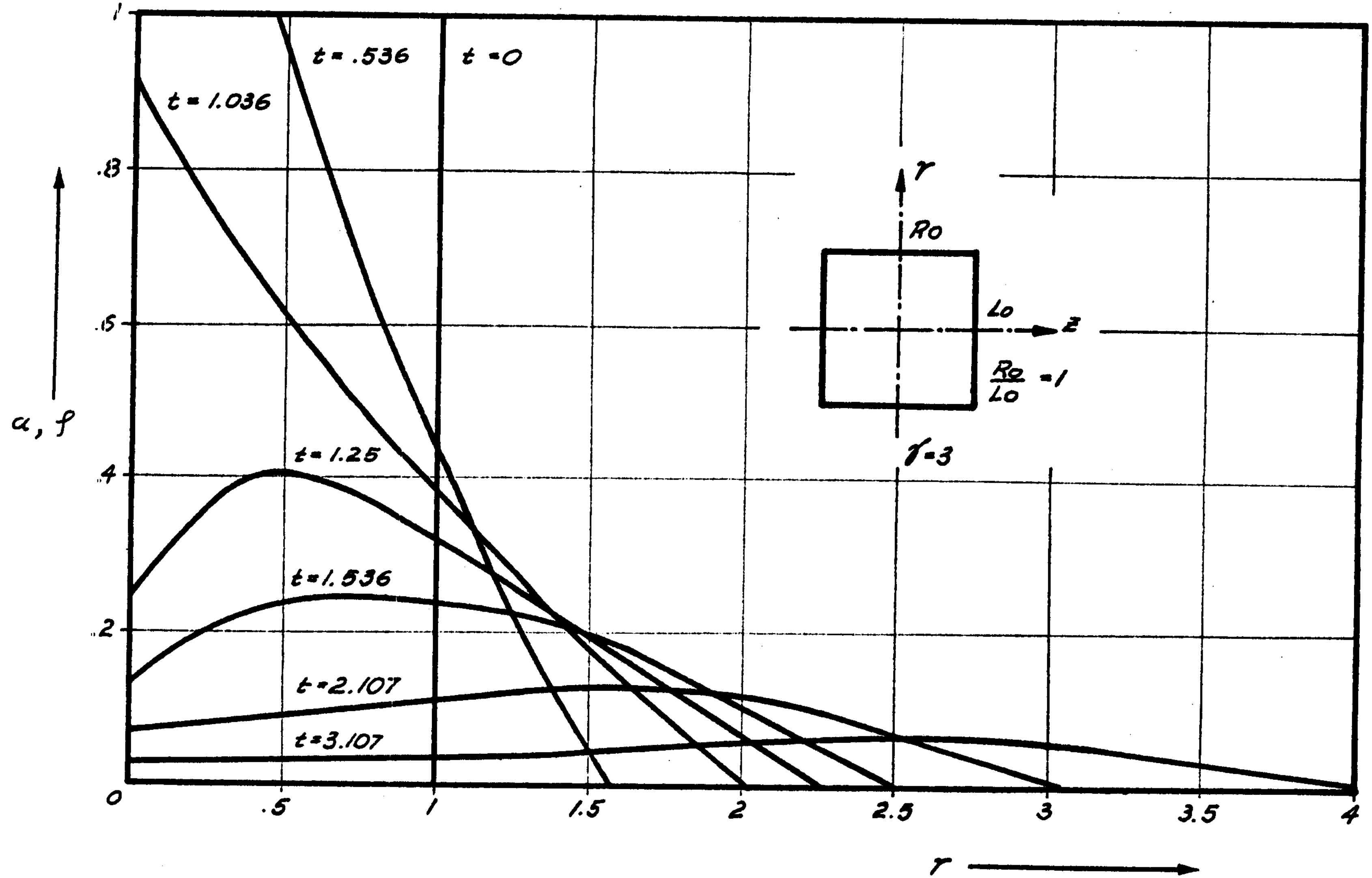

FIG. 3.6 SOUND SPEED PROFILES FOR SQUARE CYLINDER ALONG r AXIS

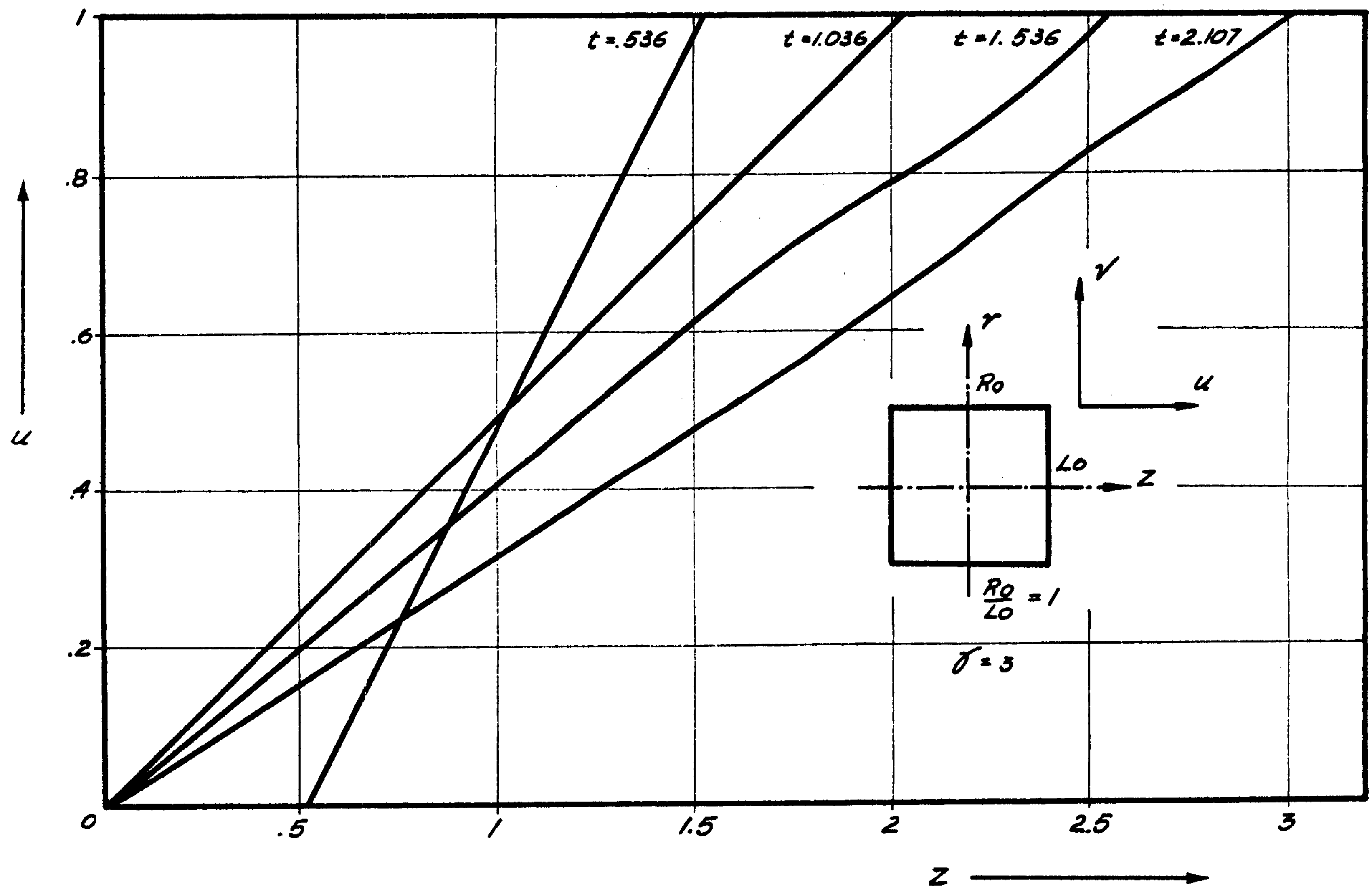

FIG. 3.7 PARTICLE VELOCITY PROFILES FOR SQUARE CYLINDER ALONG Z AXIS

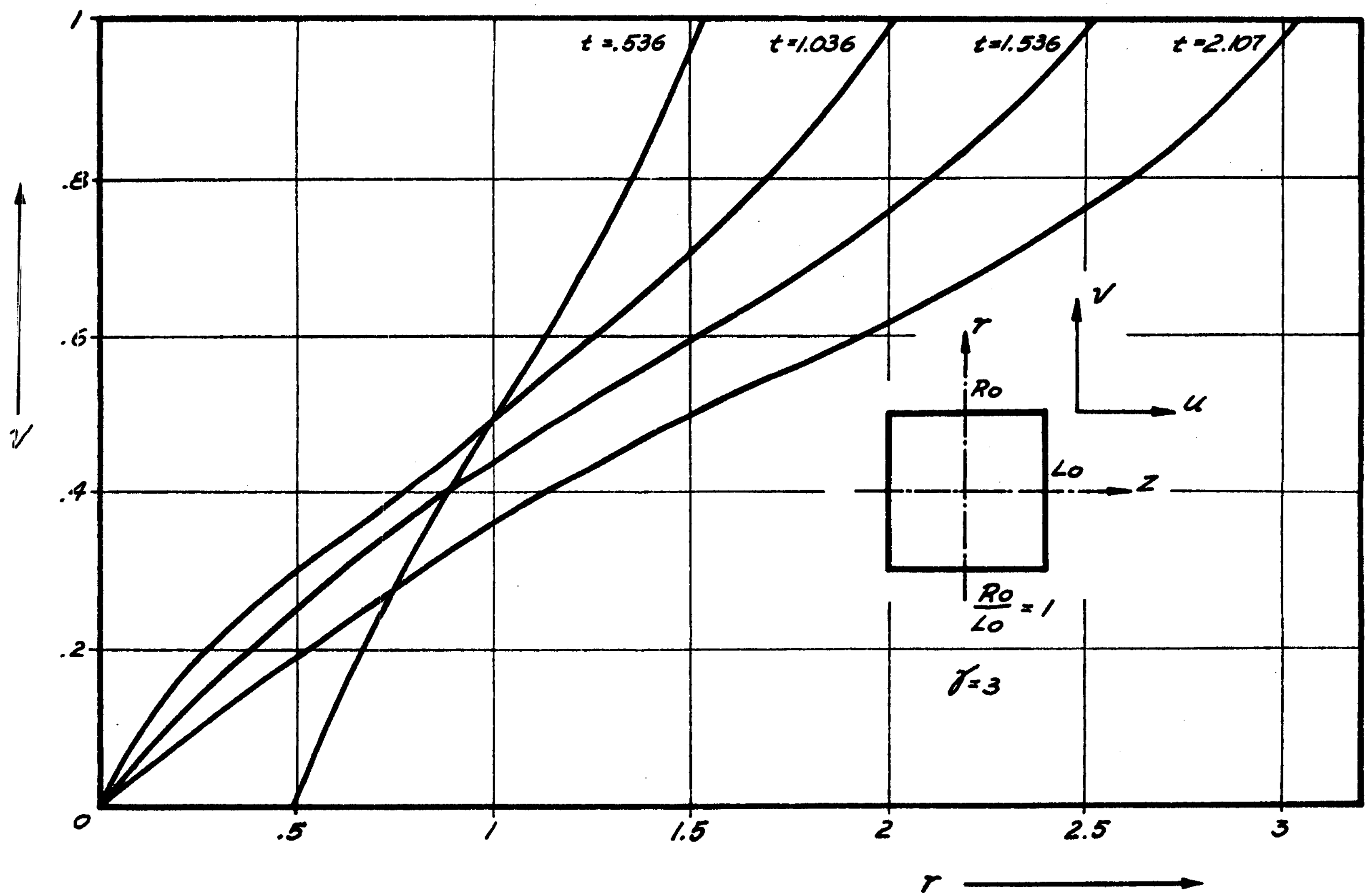

FIG. 3.8 PARTICLE VELOCITY PROFILES FOR SQUARE CYLINDER ALONG r AXIS

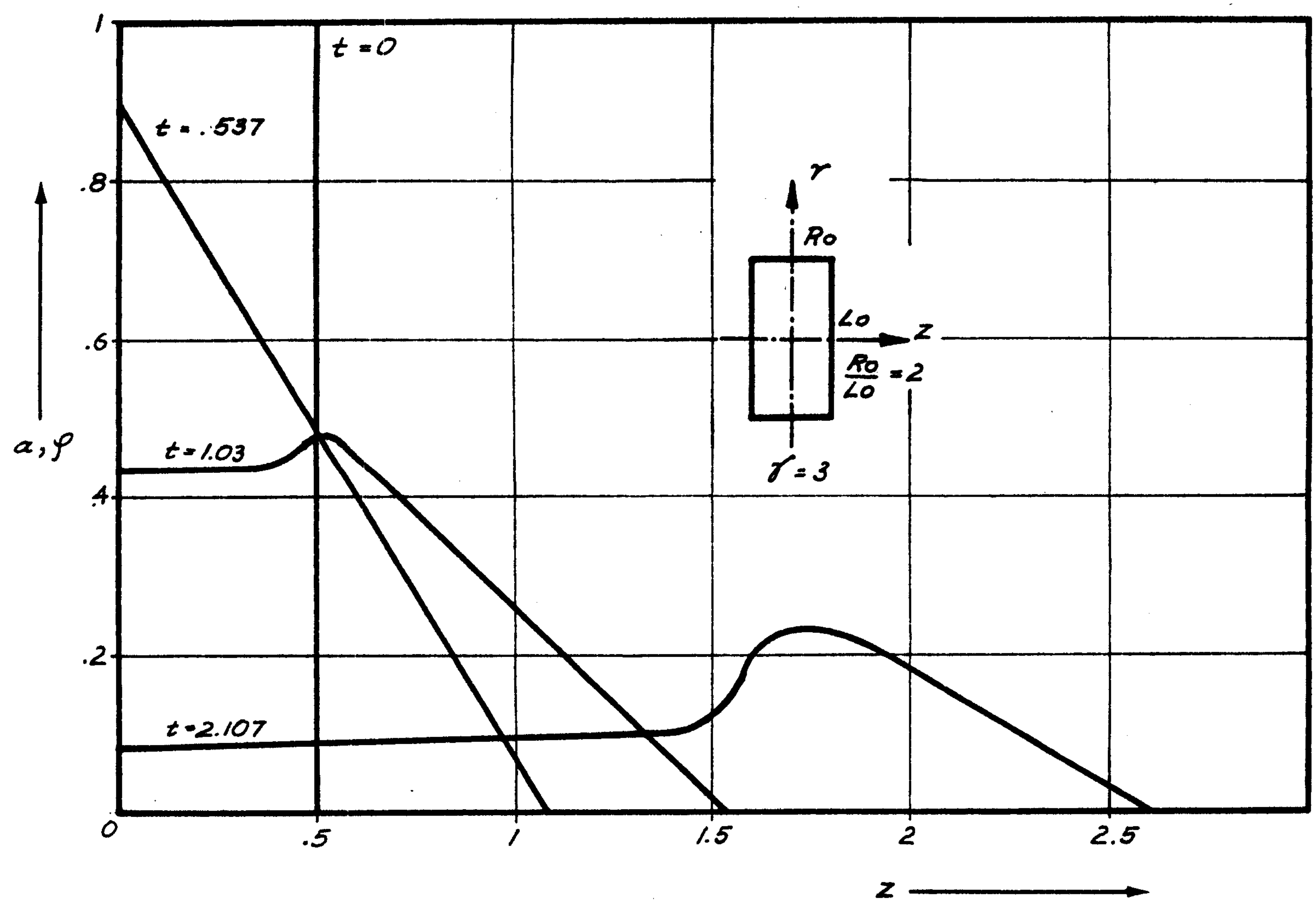

FIG. 3.9 SOUND SPEED PROFILES FOR SHORT CYLINDER ALONG Z AXIS

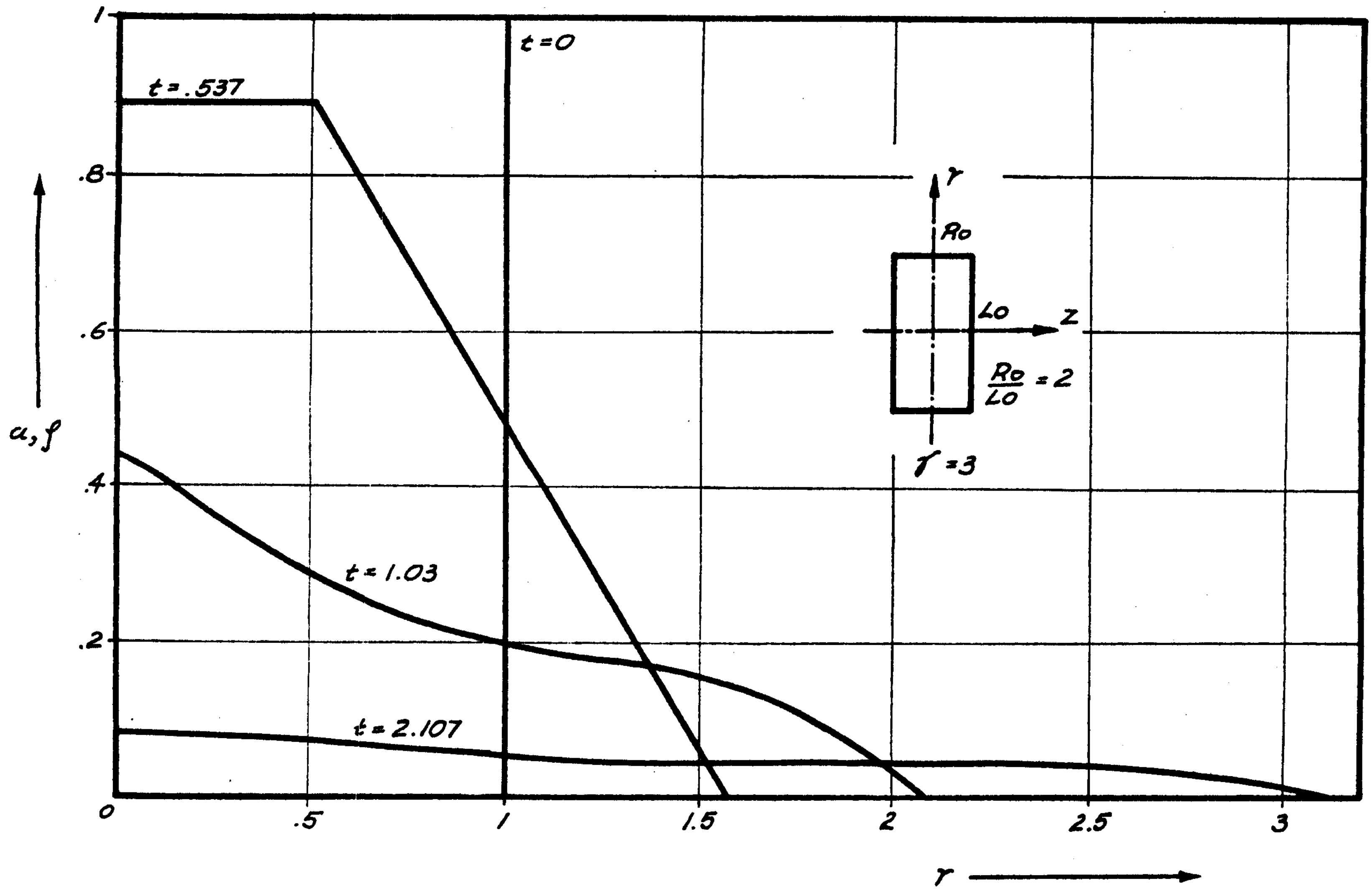

FIG. 3.10 SOUND SPEED PROFILES FOR SHORT CYLINDER ALONG r AXIS

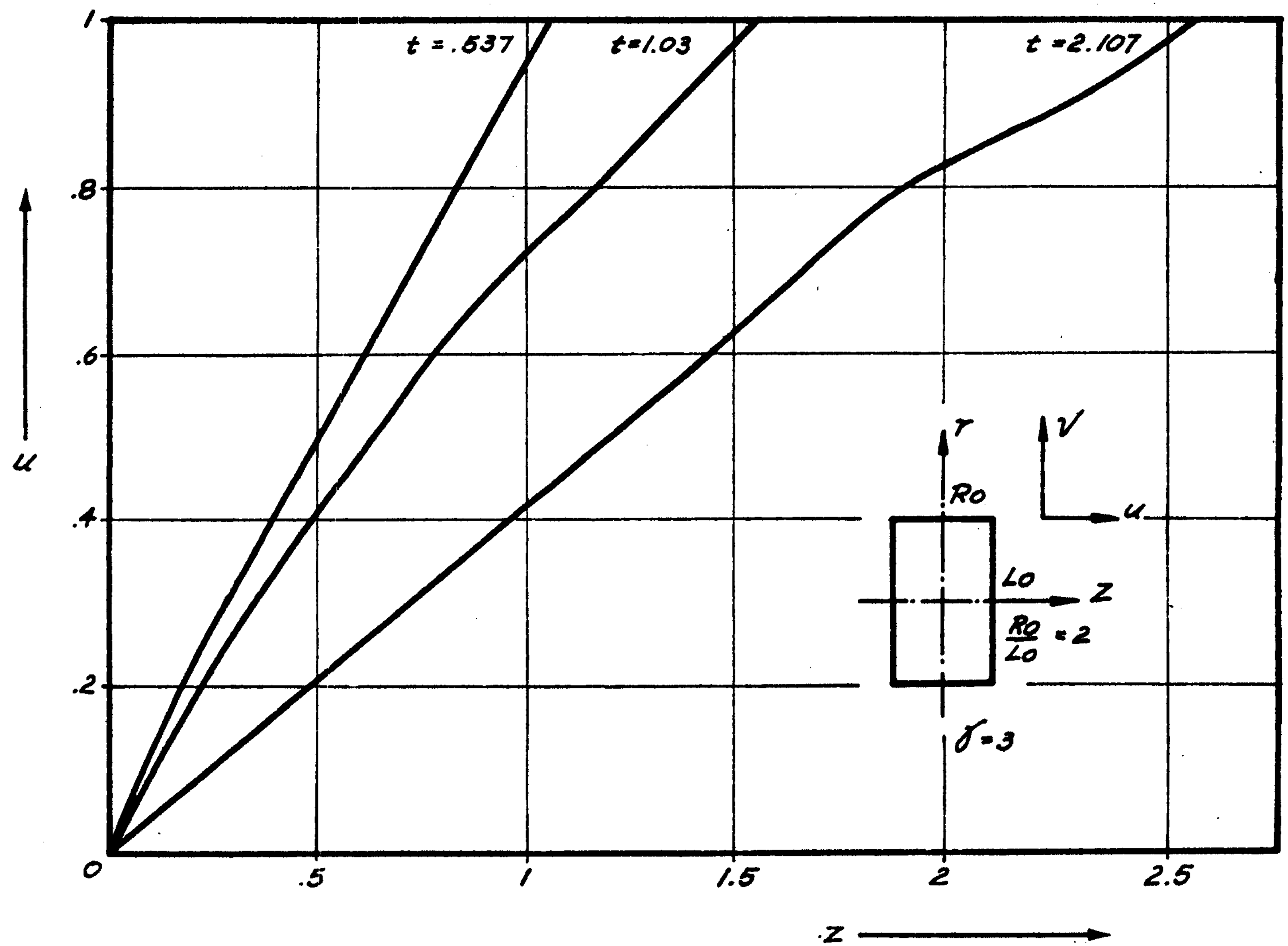

FIG. 3.11 PARTICLE VELOCITY PROFILES FOR SHORT CYLINDER ALONG Z AXIS

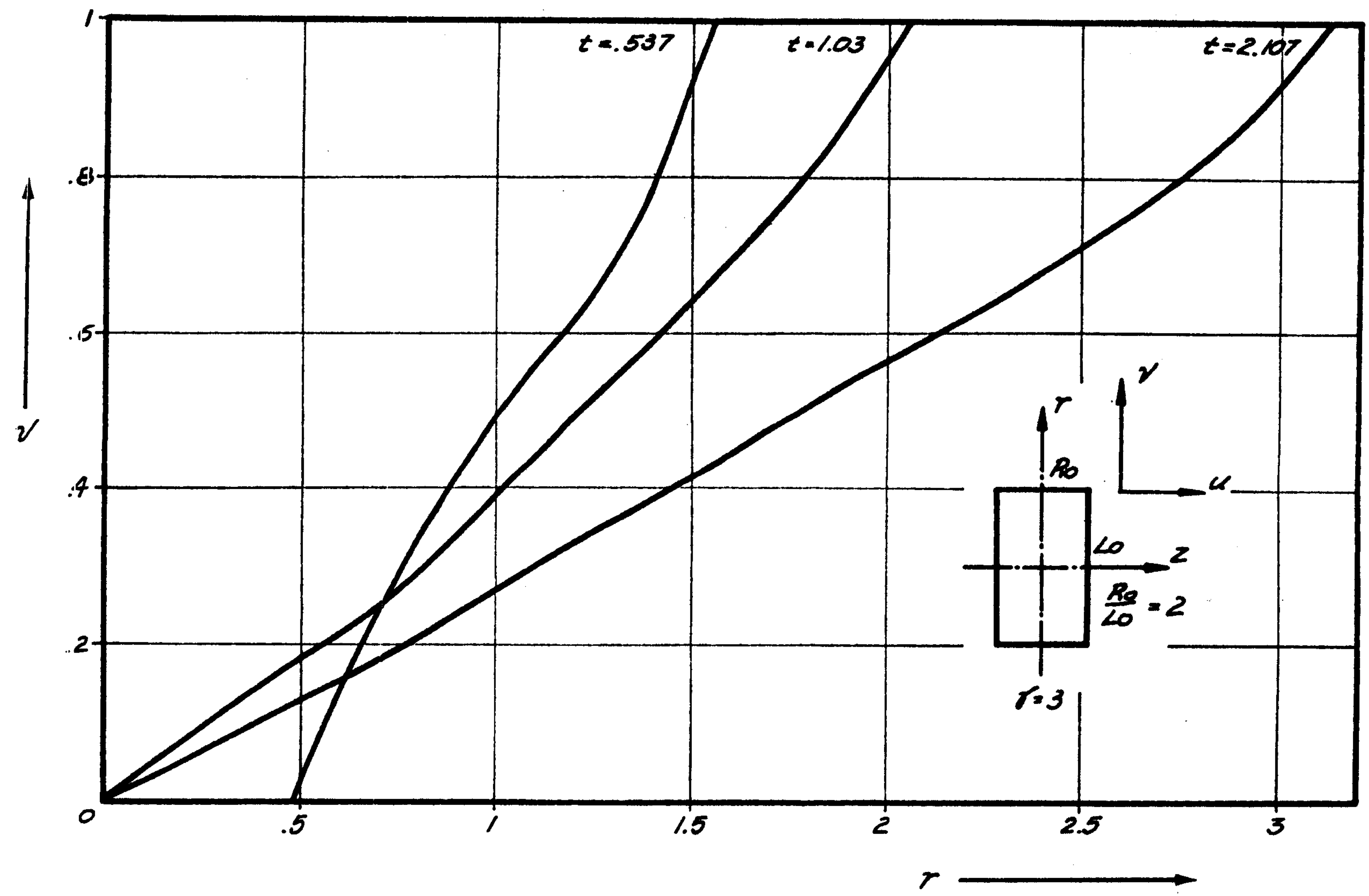

FIG. 3.12 PARTICLE VELOCITY PROFILES FOR SHORT CYLINDER ALONG r AXIS

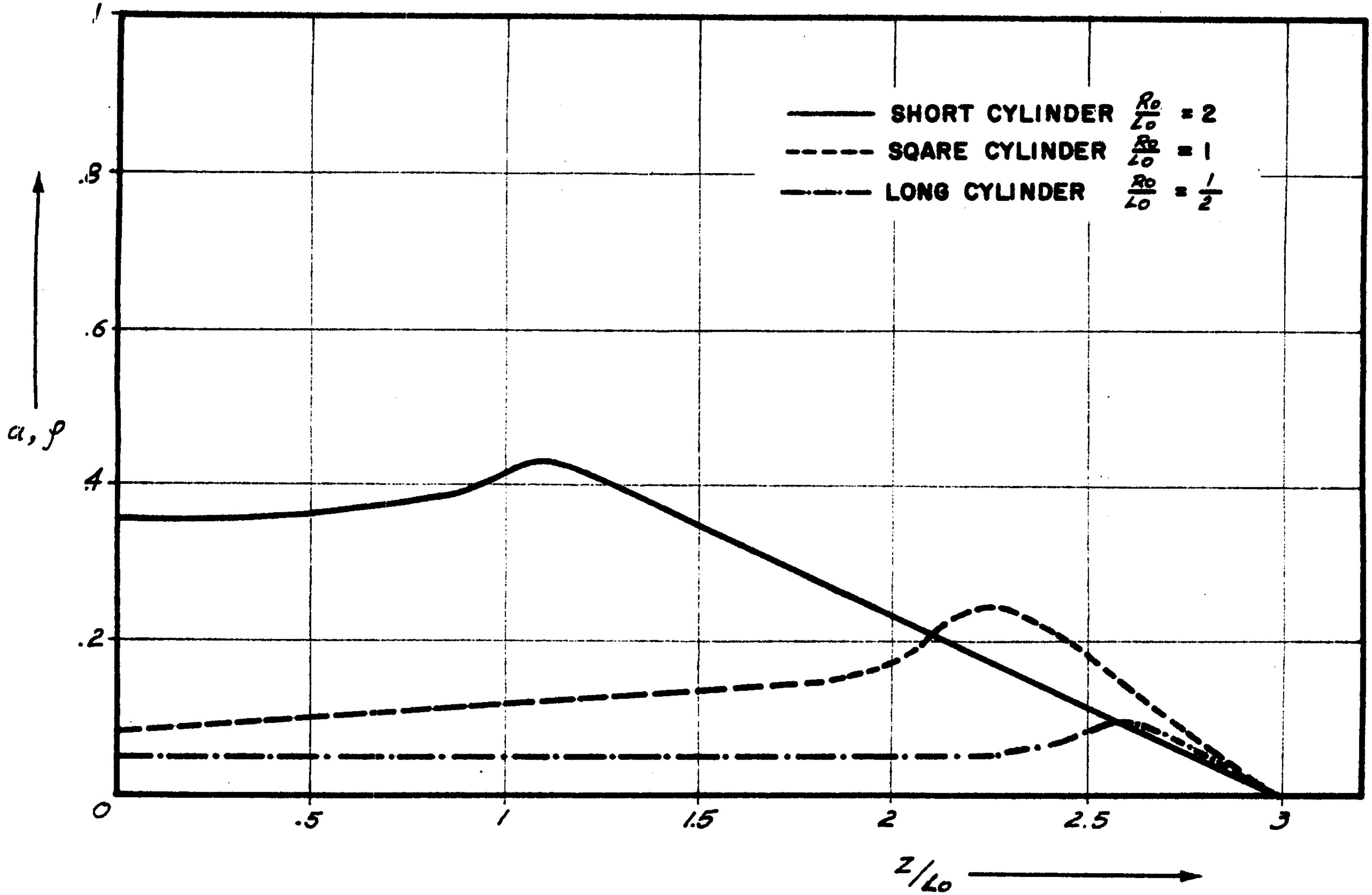

FIG. 3.13 COMPARISON OF AXIAL SOUND SPEED PROFILES FOR SQUARE, SHORT AND LONG CYLINDERS FOR ESCAPE FRONT AT $Z = 3\ L_o$

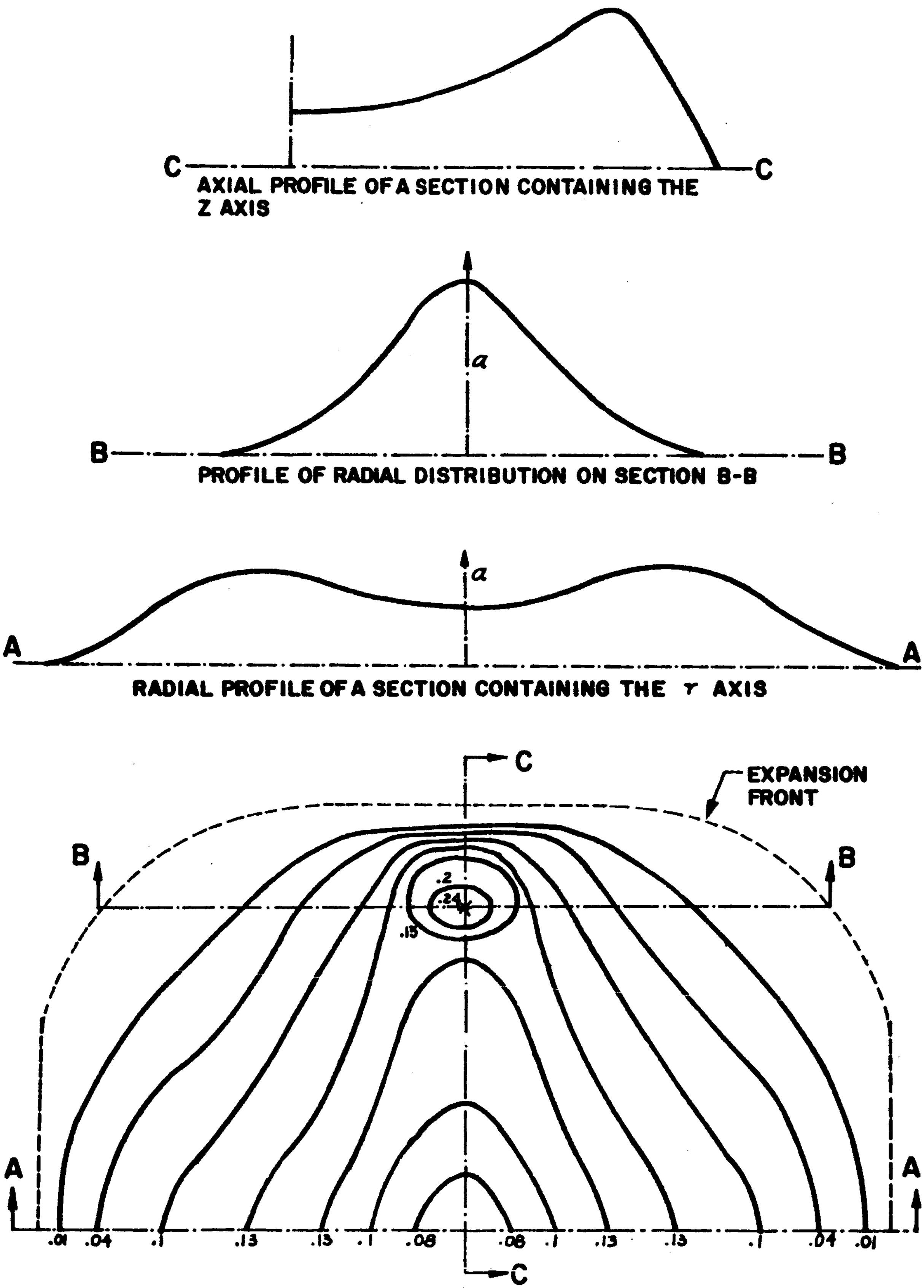

FIG. 3.14 CONSTANT DENSITY CONTOURS FOR THE SQUARE CYLINDER WHEN ESCAPE FRONT PROCEEDED OUT A DISTANCE OF 2 Ro

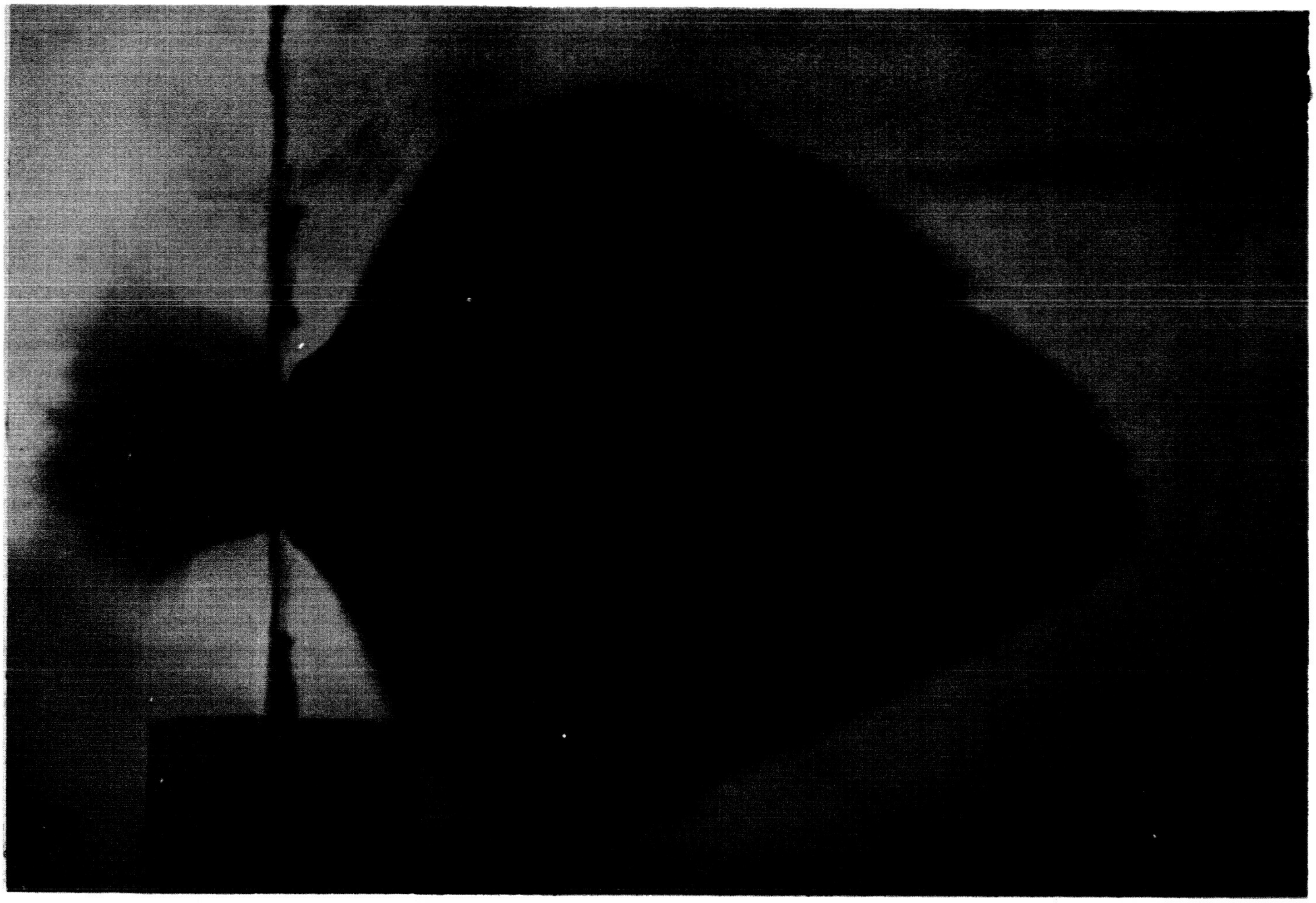

FIG. 3.15 SHADOWGRAPH OF AN EXPANDING GAS CLOUD

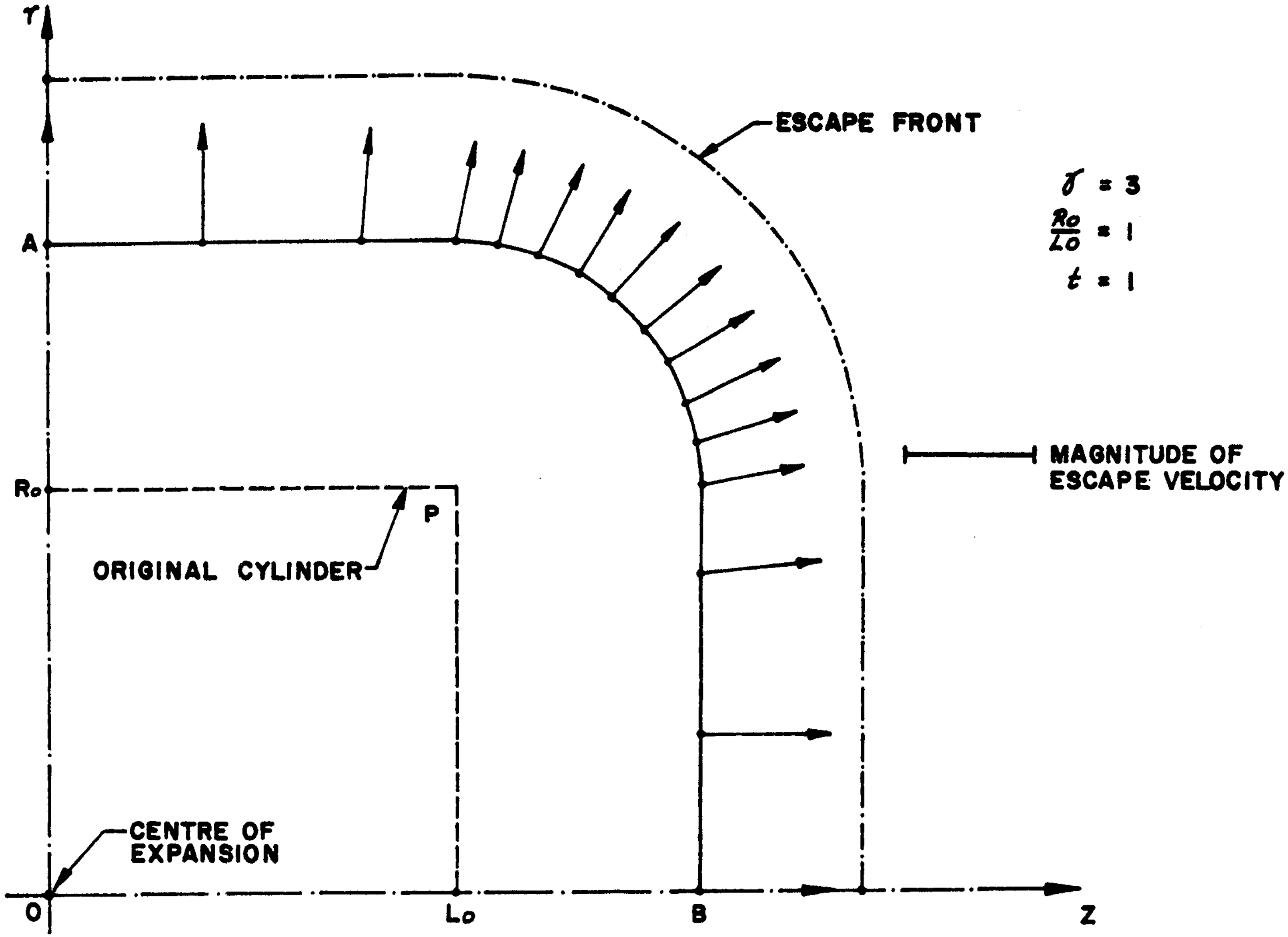

FIG. 3.16 MAGNITUDE AND DIRECTION OF THE PARTICLE VELOCITY ON A SURFACE IN THE EXPANSION FIELD

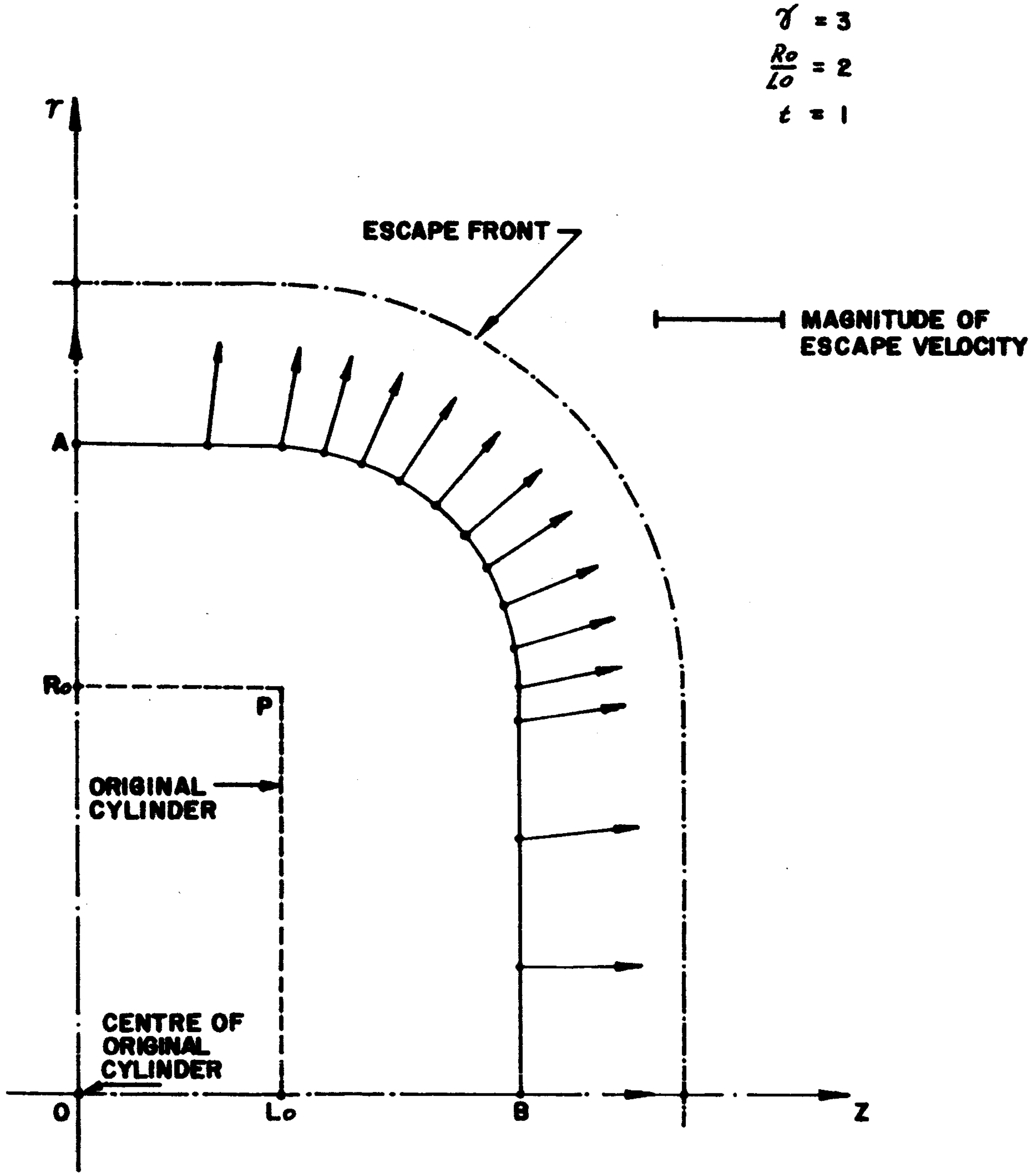

FIG. 17 MAGNITUDE AND DIRECTION OF THE PARTICLE VELOCITY ON A SURFACE IN THE EXPANSION FIELD

DISTRIBUTION LIST

		COPIES
National Aeronautics and Space Administration Lewis Research Center 21000 Brookpark Road Cleveland, Ohio 44135		
Attention:	Contracting Officer, MS 500-210	1
	Liquid Rocket Technology Branch, MS 500-209	8
	Technical Report Control Office, MS 5-5	1
	Technology Utilization Office, MS 3-16	1
	AFSC Liaison Office, MS 4-1	2
	Library	2
	Office of Reliability & Quality Assurance, MS 500-203	1
National Aeronautics and Space Administration Washington, D. C. 20546		
Attention:	Code, RV-2	2
Scientific and Technical Information Facility P. O. Box 5700 Bethesda, Maryland 20014		
Attention:	NASA Representative Code CRT	6
National Aeronautics and Space Administration Ames Research Center Moffett Field, California 94035		
Attention:	Library	1
National Aeronautics and Space Administration Flight Research Center P. O. Box 273 Edwards, California 93523		
Attention:	Library	1
National Aeronautics and Space Administration Goddard Space Flight Center Greenbelt, Maryland 20771		
Attention:	Library	1
	W.M. Alexander	1

	COPIES
National Aeronautics and Space Administration Langley Research Center Langley Station Hampton, Virginia 23365 Attention: Library	1
National Aeronautics and Space Administration Manned Spacecraft Center Houston, Texas 77001 Attention: Library	1
National Aeronautics and Space Administration George C. Marshall Space Flight Center Huntsville, Alabama 35812 Attention: Library	1
National Aeronautics and Space Administration Western Operations 150 Pico Boulevard Santa Monica, California 90406 Attention: Library	1
National Aeronautics and Space Administration John F. Kennedy Space Center Cocoa Beach, Florida 32931 Attention: Library	1
Jet Propulsion Laboratory 4800 Oak Grove Drive Pasadena, California 91103 Attention: Library	1
Office of the Director of Defense Research & Engineering Washington, D. C. 20301 Attention: Dr. H.W. Schulz, Office of Asst. Dir. (Chem. Technology)	1

	COPIES
RTD (RTNP) Bolling Air Force Base Washington, D. C. 20332	1
Attention: J. Minette,	1
E.A. Kritzer	1
Arnold Engineering Development Center Air Force Systems Command Tullahoma, Tennessee 37389	
Attention: AEOIM	1
Office of Research Analyses (OAR) Holloman Air Force Base, New Mexico 88330	
Attention: RRRT	1
Air Force Office of Scientific Research Washington, D. C. 20333	
Attention: SREP, Dr. J.F. Masi	1
Wright-Patterson Air Force Base, Ohio 45433	
Attention: AFML (MAAE)	1
AFML (MAAM)	1
Commanding Officer Ballistic Research Laboratories Aberdeen Proving Ground, Maryland 21005	
Attention: AMXBR-1	1
Department of the Army U. S. Army Materiel Command Washington, D. C. 20315	
Attention: AMCRD-RC	1
U. S. Army Missile Command Redstone Scientific Information Center Redstone Arsenal, Alabama 35808	
Attention: Chief, Document Section	1

COPIES

Bureau of Naval Weapons Department of the Navy Washington, D. C. 20360 Attention: DLI-3	1
Commander U. S. Naval Missile Center Point Mugu, California 93041 Attention: Technical Library	1
Commander U. S. Naval Ordnance Laboratory White Oak Silver Spring, Maryland 20910 Attention: Library	1
Commander (Code 753) U. S. Naval Ordnance Test Station China Lake, California 93557 Attention: Technical Library	1
Commanding Officer Office of Naval Research 1030 E. Green Street Pasadena, California 91101	1
Director (Code 6180) U. S. Naval Research Laboratory Washington, D. C. 20390	
Attention: H.W. Carhart	1
W.W. Atkins	1
M.A. Persechino	1
Commander U. S. Naval Weapons Laboratory Dahlgren, Virginia 22448 Attention: Technical Library	1
Aerojet-General Corporation P. O. Box 296 Azusa, California 91703 Attention: Librarian	1

		COPIES
Aerojet-General Corporation 11711 South Woodruff Avenue Downey, California 90241		
Attention:	F.M. West, Chief Librarian	1
	J.F. Collinane	1
Aerojet-General Corporation P. O. Box 1947 Sacramento, California 95809		
Attention:	Technical Library 2484-2015A	1
Aerospace Corporation P. O. Box 95085 Los Angeles, California 90045		
Attention:	Library-Documents	1
IIT Research Institute Technology Center Chicago, Illinois 60616		
Attention:	C.K. Hersh, Chemistry Division	1
	Dr. R.H. Cornish	1
ARO, Inc. Arnold Engrg. Dev. Center Arnold AF Station, Tennessee 37389		
Attention:	Dr. B.H. Goethert, Chief Scientist	1
	Julium Lukasiewicz	1
University of Denver Denver Research Institute P. O. Box 10127 Denver, Colorado 80210		
Attention:	Security Office	1
	R.E. Recht, Mechanics Division	1
Battelle Memorial Institute 505 King Avenue Columbus, Ohio 43201		
Attention:	Report Library, Room 6A	1

COPIES

Bell Aerosystems Box 1 Buffalo, New York 14205 Attention: T. Reinhardt	1
The Boeing Company Aero Space Division P. O. Box 3707 Seattle, Washington 98124 Attention: Ruth E. Peerenboom (1190)	1
Jack Lundeberg	1
Chemical Propulsion Information Agency Applied Physics Laboratory 8621 Georgia Avenue Silver Spring, Maryland 20910	1
Propulsion Engineering Division (D.55-11) Lockheed Missiles & Space Company 1111 Lockheed Way Sunnyvale, California 94087	1
Douglas Aircraft Company, Inc. Santa Monica Division 3000 Ocean Park Boulevard Santa Monica, California 90405 Attention: J.L. Waisman	1
General Dynamics/Astronautics P. O. Box 1128 San Diego, California 92112 Attention: Library and Information Services (128-00)	1
Institute for Defense Analyses 400 Army-Navy Drive Arlington, Virginia 22202 Attention: Classified Library	1

	COPIES
Lockheed Propulsion Company P. O. Box 111 Redlands, California 92374	
Attention: Miss Belle Berlad, Librarian	1
Marquardt Corporation 16555 Saticoy Street Box 2013 - South Annex Van Nuys, California 91404	1
North American Aviation, Inc. Space & Information Systems Division 12214 Lakewood Boulevard Downey, California 90242	
Attention: Technical Information Center	1
D/096-722 (AJ01) E.R. Mertz	1
Rocketdyne 6633 Canoga Avenue Canoga Park, California 91304	
Attention: Library, Department 596-306	1
Rocket Research Corporation 520 South Portland Street Seattle, Washington 98108	1
Space Technology Laboratory, Inc. 1 Space Park Redondo Beach, California 90200	
Attention: STL Tech. Lib. Doc. Acquisitions	2
United Aircraft Corporation Corporation Library 400 Main Street East Hartford, Connecticut 06118	
Attention: Dr. David Rix	1

	COPIES
United Aircraft Corporation United Technology Center P. O. Box 358 Sunnyvale, California 94088	
Attention: Librarian	1
General Electric Company Apollo Support Department P. O. Box 2500 Daytona Beach, Florida 32015	
Attention: C. Day	1
National Aeronautics and Space Administration Langley Research Center Langley Station Hampton, Virginia 23365	
Attention: D. Davis, Jr.	1
J.R. Dawson	1
Richard Heldenfels	1
William Kinard	1
E.T. Kruszewski	1
R.S. Osborne	1
Jerry Williams	1
National Aeronautics and Space Administration Ames Research Center Moffett Field, California	
Attention: Donald E. Gault	1
C. Robert Nysmith	1
James L. Summers	1
National Aeronautics and Space Administration George C. Marshall Space Flight Center Huntsville, Alabama	
Attention: Research Projects Div. (M-RP-R)	1
Jose F. Blumerick	1
James W. Carter, Future Projects Office, MFPO	1
Orlo K. Hudson	1
W.G. Johnson	1
W.D. Morphree	1

COPIES

National Aeronautics and Space Administration Manned Spacecraft Center Houston, Texas	
Attention: Paige B. Burbank	1
C.R. Perrine	1
L.G. St. Leger	1
Jet Propulsion Laboratory 4800 Oak Drive Pasadena 2, California	
Attention: Charles Campen	1
Dr. V. Jaffe	1
C.L. Robillard	1
Dwayne F. Spencer	1
Wright-Patterson A. F. B. Ohio	
Attention: Commander, Air Tech. Intelligence Center Attention: F. Sachleh	1
University of California Los Alamos Scientific Laboratory P. O. Box 1663 Los Alamos, New Mexico	1
Prof. Pei Chi Chou Dept. of Mechanical Engineering Drexel Institute of Technology Philadelphia 4, Pennsylvania	1
New York University College of Engineering Research Division University Heights New York 53, New York	
Attention: Dr. Paul F. Winternite	1
Harvard College Observatory Cambridge, Massachusetts	
Attention: Prof. F.L. Whipple	1

	COPIES
Cornell Aeronautical Laboratory, Inc. Buffalo, New York	
Attention: Dr. William Rae	1
Rand Corporation Santa Monica, California	
Attention: Robert A. Popetti	1
James Rosen	1
Jack E. Whitener	1
Aero-Space Corporation El Segundo, California	
Attention: Verne C. Frost	1
University of Toronto Toronto, Canada	
Attention: I.I. Glass	1
Sandia Corporation Albuquerque, New Mexico	
Attention: Walter Herrmann	1
Arthur D. Little, Inc. Cambridge 40, Massachusetts	
Attention: Reed H. Johnston	1
Martin Company P. O. Box 179 Denver, Colorado	
Attention: Dr. Arthur Ezra	1
Avco Corporation Wilmington, Massachusetts 01887	
Attention: Robert R. McMath - RAD	1

	COPIES
Chance Vought Corporation Library Box 5907 Dallas 22, Texas	1
Chrysler Corporation P. O. Box 26018 New Orleans 26, La.	
Attention: Elayne M. Brower - AEB-2761	1
Fundamental Methods Associates 31 Union Square West New York 2, New York	
Attention: Dr. Carl Klahr	1
General Electric Valley Forge Space Tech. Center P. O. Box 8555 Philadelphia 1, Pennsylvania	
Attention: T.D. Riney - TEMO J.F. Heyda - TEMO	1 1
General Motors Defense Research Labs Santa Barbara, California	
Attention: C.J. Maiden	1
Gruman Aircraft Engineering Corporation Bethpage, Long Island New York	
Attention: Library John Tlasmati	1 1
Lockheed Missiles and Space Company Palo Alto, California	
Attention: P.E. Sandorff	1
The Martin Company Science Technology Library Mail 398 Baltimore 3, Maryland	1

	COPIES
Northrop Space Laboratories 3401 West Broadway Hawthrone, California 90250	
Attention: R.D. Johnson, Space Materials Lab.	1
Republic Aviation Corporation Farmingdale, Long Island New York	
Attention: Sol Saul, Space System Structures	1
Utah Research and Development 2175 South 3270 West Salt Lake City, Utah	
Attention: Boyd Baugh	1
Computing Devices of Canada Limited P. O. Box 508 Ottawa 4, Canada	
Attention: Dr. G.P.T. Wilenius	2
Republic Aviation 333 West 1st Street Dayton 2, Ohio	
Attention: Paul Rossow	1
Lockheed Missiles and Space Company Building 102 Sunnyvale, California 94087	
Attention: R.L. Hammitt, Dept. 55-23	1
Canadian Commercial Corporation 70 Lyon Street Ottawa, Canada	
Attention: J.A. Given - Machinery Branch	1